International Telecommunication Union

ITU-R

Radiocommunication Sector of ITU

Recommendation ITU-R P.2040

(09/2013)

Effects of building materials and structures on radiowave propagation above about 100 MHz

P Series

Radiowave propagation

International Telecommunication Union

Foreword

The role of the Radiocommunication Sector is to ensure the rational, equitable, efficient and economical use of the radio-frequency spectrum by all radiocommunication services, including satellite services, and carry out studies without limit of frequency range on the basis of which Recommendations are adopted.

The regulatory and policy functions of the Radiocommunication Sector are performed by World and Regional Radiocommunication Conferences and Radiocommunication Assemblies supported by Study Groups.

Policy on Intellectual Property Right (IPR)

ITU-R policy on IPR is described in the Common Patent Policy for ITU-T/ITU-R/ISO/IEC referenced in Annex 1 of Resolution ITU-R 1. Forms to be used for the submission of patent statements and licensing declarations by patent holders are available from http://www.itu.int/ITU-R/go/patents/en where the Guidelines for Implementation of the Common Patent Policy for ITU-T/ITU-R/ISO/IEC and the ITU-R patent information database can also be found.

Series of ITU-R Recommendations

(Also available online at http://www.itu.int/publ/R-REC/en)

Series	Title
BO	Satellite delivery
BR	Recording for production, archival and play-out; film for television
BS	Broadcasting service (sound)
BT	Broadcasting service (television)
F	Fixed service
M	Mobile, radiodetermination, amateur and related satellite services
P	**Radiowave propagation**
RA	Radio astronomy
RS	Remote sensing systems
S	Fixed-satellite service
SA	Space applications and meteorology
SF	Frequency sharing and coordination between fixed-satellite and fixed service systems
SM	Spectrum management
SNG	Satellite news gathering
TF	Time signals and frequency standards emissions
V	Vocabulary and related subjects

Note: *This ITU-R Recommendation was approved in English under the procedure detailed in Resolution ITU-R 1.*

Electronic Publication
Geneva, 2013

RECOMMENDATION ITU-R P.2040

Effects of building materials and structures on radiowave propagation above about 100 MHz

(Question ITU-R 211/3)

(2013)

Scope

This Recommendation provides guidance on the effects of building material properties and structures on radiowave propagation. Basic principles and building loss measurements affected by building materials and structures are also discussed.

The ITU Radiocommunication Assembly,

considering

a) that electrical properties of materials and their structures strongly affect radiowave propagation;

b) that it is necessary to understand the losses of radiowaves caused by building materials and structures;

c) that there is a need to give guidance to engineers to avoid interference from outdoor to indoor and indoor to outdoor systems;

d) that there is a need to provide users with a unified source for computing effects of building materials and structures,

noting

a) that Recommendation ITU-R P.679 provides guidance on planning broadcasting-satellite systems;

b) that Recommendation ITU-R P.1238 provides guidance on indoor propagation over the frequency range 900 MHz to 100 GHz;

c) that Recommendation ITU-R P.1406 provides information on various aspects of propagation relating to terrestrial land mobile and broadcasting services in the VHF and UHF bands;

d) that Recommendation ITU-R P.1411 provides propagation methods for short paths in outdoor situations, in the frequency range from about 300 MHz to 100 GHz,

recommends

that the information and methods in Annex 1 should be used as a guide for the assessment on the effects of building material properties and structures on radiowave propagation loss.

Annex 1

1 Introduction

The purpose of this Recommendation is to provide guidance on the effects of building material electrical properties and structures on radiowave propagation. This task will be accomplished in three parts. The first part, the Introduction, will provide a high-level discussion of outdoor-indoor and indoor-outdoor propagation scenarios and definitions of some relevant terms. The second part will provide detailed quantitative theoretical results for electromagnetic plane wave interactions with lossy half-planes, slabs, scattering objects, apertures and other structures, in order to elucidate the dependences on material property values, frequency, angle of incidence and polarization. In addition, results from the theory of waveguides and resonant cavities forming the boundaries in separable coordinate systems will be considered. The second part will also provide results from the theory of the electrical/magnetic properties of materials, in order to promote understanding of the frequency (and other) dependences of material electrical/magnetic properties. Finally, the third part will provide methods for measuring and reporting material properties, along with compilations of common building material measured properties. The document will provide the user with a unified source for computing the effects of building materials and structures on system performance.

1.1 Description of scenarios

1.1.1 Outside-inside propagation: issues concerning entry-loss reference field

A difficulty with defining the entry loss reference field is that the presence of the building will modify signal strengths outside it. Figure 1 illustrates, in somewhat simplified form, the issues involved. The three sections of the figure show:

a) A relatively isolated outdoor point receives a direct and ground-reflected ray. In fact both of these rays, in an urban environment, may well arrive from a distant source via diffraction over a building to the left of the figure. For propagation at small angles to the horizontal, there will be fairly simply and mainly vertical lobing, that is, maxima and minima when the point is moved vertically.

b) Without moving the point, a building is placed just behind it. It now receives two additional rays reflected from the building, one of which is also ground-reflected. The lobing pattern will now have fine structure in both the vertical and horizontal directions.

c) The point is now moved inside the building. For the purposes of illustration the frequency is assumed to be high enough such that only rays entering a window are significant. At a lower frequency, where penetration through the wall is significant, the ray pattern would change.

FIGURE 1

Simplified ray diagrams for outdoor and indoor points

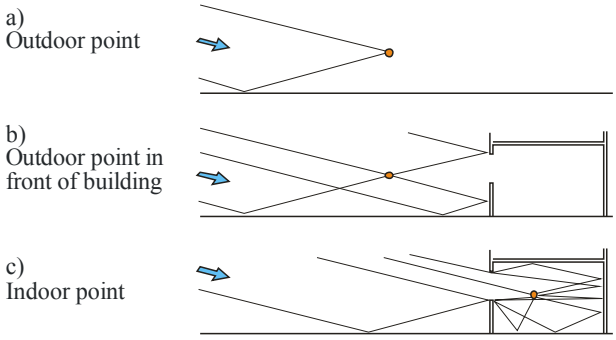

Although multipath propagation causes lobing, the power-sum of multiple rays approximates to the spatially-averaged field. In general, therefore, the presence of a building behind a receiver can be expected to increase the received signal strength. Inside the building, particularly close to the illuminated external wall, a larger number of rays is likely to be received, although many will be attenuated by transmission, reflection or diffraction. It is thus possible to have a stronger signal inside than outside.

1.1.2 Building propagation loss

Figure 2 shows the different kinds of building losses encountered in an outdoor-indoor and indoor-outdoor scenario. The definitions are given in the next sections.

FIGURE 2

Different kinds of building propagation loss

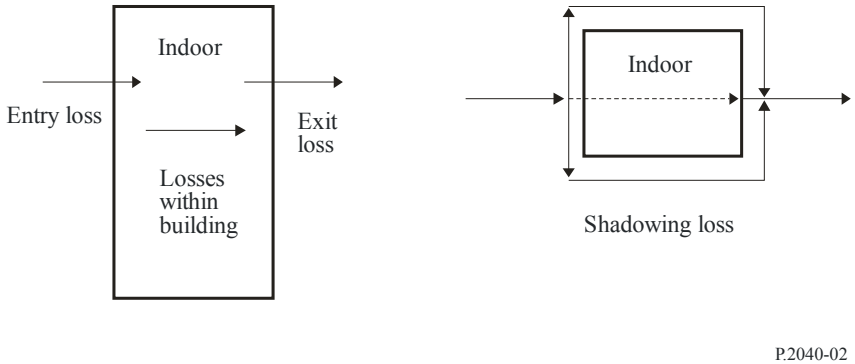

1.2 Definition of building entry loss

The building entry loss is the difference between the spatial median of the signal level outside the illuminated face of a building and the signal level inside the building at the same height above ground, with multipath fading spatially averaged for both signals.

1.3 Definition of building shadowing loss

The building shadowing loss is the difference between the median of the location variability of the signal level outside the illuminated face of a building and the signal level outside the opposite face

of the building at the same height above ground, with multipath fading spatially averaged for both signals. It can be considered as the transmission loss through a building.

1.4 Definition of (e.g. wall) penetration

Signals outside a building enter an enclosed building by penetration mostly through walls. Wall penetration can also refer to the penetration through partitions inside buildings. Inside buildings, wall penetration loss is the difference between the median of the location variability of the signal level on one side of a wall, and the signal level on the opposite side of the wall at the same height above ground, with multipath fading spatially averaged for both signals. It can be considered as the transmission loss through a wall.

1.5 Definition of aperture penetration

Aperture penetration is the penetration of signals from one side of a wall to the other side through openings on the walls like windows.

1.6 Definition of building exit loss

The building exit loss, which is the reverse definition of building entry loss, is the difference between the median of the location variability of the signal level inside the illuminated face of a building and the signal level outside the building at the same height above ground, with multipath fading spatially averaged for both signals.

2 Basic principles and theory

Radiowaves that interact with a building will produce losses that depend on the electrical properties of the building materials and material structure. In this section, theoretical effects of material electrical properties and structure on radiowave propagation will be discussed.

2.1 Theory of material electrical properties

2.1.1 Introduction

This section describes the development of simple frequency-dependent formulae for the permittivity and conductivity of common building materials. The formulae are based on curve fitting to a number of published measurement results, mainly in the frequency range 1-100 GHz. The aim is to find a simple parameterization for use in indoor-outdoor ray trace modelling.

The characterization of the electrical properties of materials is presented in a number of different ways in the literature. These are described in § 2.1.2 in order that the measured data can be reduced to a common format.

2.1.2 Method

2.1.2.1 Definitions of electrical constants

The method only deals with non-ionized, non-magnetic materials, and throughout we therefore set the free charge density, ρ_f, to zero and the permeability of the material, μ, to the permeability of free space μ_0.

The fundamental quantities of interest are the electrical permittivity, ε, and the conductivity, σ. There are many ways of quantifying these parameters in the literature, so we first make explicit these different representations and the relations between them.

2.1.2.2 Derivation

The starting point is the wave equation derived from Maxwell's equations. Under the above assumptions, the wave equation for the electric field $\vec{E}$ is:

$$\nabla^2 \vec{E} - \varepsilon\mu_0 \frac{\partial^2 \vec{E}}{\partial t^2} = \mu_0 \frac{\partial \vec{J}_f}{\partial t} \tag{1}$$

where:

$\vec{E}$: (vector) electric field intensity (V/m)

J_f : current density of free charges (A/m^2)

ε : dielectric permittivity (F/m)

μ_0 : permeability of free space (N/A^2) = $4\pi \times 10^{-7}$ by definition.

In a conductor, $\vec{J}_f$ is related to $\vec{E}$ through Ohm's Law by:

$$\vec{J}_f = \sigma\vec{E} \tag{2}$$

where:

σ : conductivity (S/m).

Combining equations (1) and (2) gives:

$$\nabla^2 \vec{E} - \varepsilon\mu_0 \frac{\partial^2 \vec{E}}{\partial t^2} = \mu_0\sigma \frac{\partial \vec{E}}{\partial t} \tag{3}$$

Writing $\vec{E}$ in exponential notation:

$$\vec{E} = \vec{E}_0 e^{j\left(\omega t - \vec{k}\cdot\vec{r}\right)} \tag{4}$$

where:

$\vec{E}_0$: value of $\vec{E}$ for $t = \vec{r} = 0$ (V/m)

$\vec{k}$: (vector) wave number (m^{-1}) magnitude = $2\pi/\lambda$ where λ is the wavelength in m

ω : angular frequency (s^{-1}) = $2\pi f$ where f is the frequency in s^{-1}

and substituting in equation (3) gives

$$k^2 - \varepsilon\mu_0\omega^2 + j\omega\mu_0\sigma = 0 \tag{5}$$

where k is the magnitude of $\vec{k}$.

Equation (5) shows that the electric field intensity propagates as an attenuated sinusoidal wave.

2.1.2.3 Non-conducting dielectric

In a non-conducting dielectric ($\sigma = 0$) the field is unattenuated and from equation (5) the velocity of propagation, v (= ω/k), is:

$$v = \frac{1}{\sqrt{\varepsilon\mu_0}} \tag{6}$$

ε is conventionally written in terms of the relative permittivity, ε_r, and the permittivity of free space, ε_0, as:

$$\varepsilon = \varepsilon_r \, \varepsilon_0 \tag{7}$$

from which the velocity of propagation is:

$$v = \frac{c}{\sqrt{\varepsilon_r}} \tag{8}$$

c is the velocity of light in free space (= $1/\sqrt{\varepsilon_0\mu_0}$). In other words, $\sqrt{\varepsilon_r}$ is the refractive index of the dielectric medium.

2.1.2.4 Conducting dielectric

When $\sigma \neq 0$, the wave attenuates as it propagates. We can extend equation (8) to include this case by defining a complex relative permittivity ε_r^c by equation (8), with $v = \omega/k$ given more generally by equation (5):

$$\varepsilon_r^c = \varepsilon_r - j\frac{\sigma}{\varepsilon_0\omega} \tag{9}$$

This shows that the relative permittivity, ε_r (defined for a pure dielectric) becomes the real part of the more general, complex relative permittivity ε_r^c defined for a conducting dielectric. One problem is that there are no universally accepted symbols for these terms, and the literature contains a number of different definitions. The symbol ε_r itself is sometimes used for the complex relative permittivity, and sometimes for its real part.

To avoid this ambiguity, we will write ε_r^c in the form:

$$\varepsilon_r^c = \varepsilon_r^{'} - j\varepsilon_r^{''} \tag{10}$$

and use the symbol ε_r^c for complex relative permittivity and $\varepsilon_r^{'}$ for its real part, avoiding the use of the symbol ε_r. Using equation (9), the imaginary part of ε_r^c is simply:

$$\varepsilon_r^{''} = \frac{\sigma}{\varepsilon_0\omega} \tag{11}$$

Note that the sign of the imaginary part of ε_r^c is arbitrary, and reflects our sign convention in equation (4). In practical units, equation (9) gives a conversion from $\varepsilon_r^{''}$ to σ:

$$\sigma = 0.05563\varepsilon_r^{''} f_{\mathrm{GHz}} \tag{12}$$

Another formulation of the imaginary part of ε_r^c is in terms of the *loss tangent*, defined as:

$$\tan\delta = \frac{\varepsilon_r''}{\varepsilon_r'} \tag{13}$$

and so:

$$\tan\delta = \frac{\sigma}{\varepsilon\omega} \tag{14}$$

From equation (10) this gives immediately:

$$\varepsilon_r^c = \varepsilon_r'(1 - j\tan\delta) \tag{15}$$

and in practical units:

$$\sigma = 0.05563\varepsilon_r' \tan\delta\, f_{\mathrm{GHz}} \tag{16}$$

Another term sometimes encountered is the Q of the medium. This is defined as:

$$Q = \frac{\varepsilon\omega}{\sigma} \tag{17}$$

and is the ratio of the displacement current density $\partial D/\partial t$ to the conduction current density J_f. For non-conductors, $Q \to \infty$. From equations (14):

$$Q = 1/\tan\delta \tag{18}$$

Yet another term encountered is the complex refractive index n^c which is defined to be $\sqrt{\varepsilon_r^c}$. Writing n^c in terms of its real and imaginary parts:

$$n^c = n' - jn'' = \sqrt{\varepsilon_r^C} \tag{19}$$

ε_r', ε_r'' and σ are given from equations (10) and (12) by:

$$\begin{aligned} \varepsilon_r' &= (n')^2 - (n'')^2 \\ \varepsilon_r'' &= 2n'n'' \\ \sigma &= 0.1113\, n'n''\, f_{\mathrm{GHz}} \end{aligned} \tag{20}$$

2.1.2.5 Attenuation rate

A conducting dielectric will attenuate electromagnetic waves as they propagate. To quantify this, substitute equation (5) in equation (4) and simplify using equations (14):

$$\vec{E} = \vec{E}_0 \exp\left\{ j\left(\omega t - \sqrt{\varepsilon_r^{'}(1 - j\tan\delta)}\vec{k}_0 \cdot \vec{r} \right) \right\} \tag{21}$$

where:

$\vec{k}_0$: (vector) wave number (m^{-1}) in free space.

The imaginary part under the square root sign leads to an exponential decrease of the electric field with distance:

$$\vec{E} \propto \vec{E}_0 \exp\left(-|\vec{r}|/\Delta \right) \tag{22}$$

A little algebra shows that the attenuation distance, Δ, at which the field amplitude falls by $1/e$ is:

$$\Delta = \frac{1}{k_0\sqrt{\varepsilon_r^{'}}} \sqrt{\frac{2\cos\delta}{(1-\cos\delta)}} \tag{23}$$

This can be evaluated by calculating $\tan\delta$ from $\varepsilon_r^{'}$ and σ and inverting to obtain $\cos\delta$. However, a more direct evaluation is possible in the two limits of $\sigma \to 0$ (dielectric limit) and $\sigma \to \infty$ (good conductor limit). By choosing the appropriate approximation of the term under the square root sign in equations (21) these limits are:

$$\Delta_{dielectric} = \frac{1}{k_0\sqrt{\varepsilon_r^{'}}} \frac{2}{\tan\delta} \tag{24}$$

and:

$$\Delta_{conductor} = \frac{1}{k_0\sqrt{\varepsilon_r^{'}}} \sqrt{\frac{2}{\tan\delta}} \tag{25}$$

Equations (24) and (25) are accurate to about 3% for $\tan\delta < 0.5$ (dielectric) $\tan\delta > 15$ (conductor). $\Delta_{conductor}$ is usually referred to as the "skin depth".

For practical purposes the attenuation rate is a more useful quantity than the attenuation distance, and is related to it simply by

$$A = \frac{20\log_{10} e}{\Delta} = 8.686/\Delta \tag{26}$$

where:

A : attenuation rate in dB/m (with Δ in m).

Substituting equations (24) and (25) in equation (26) and converting to practical units gives:

$$A_{dielectric} = 1636 \frac{\sigma}{\varepsilon_r'} \qquad A_{conductor} = 545.8 \sqrt{\sigma f_{GHz}} \tag{27}$$

2.1.3 Frequency dependence of material properties

In the literature, the real part of the dielectric constant, ε_r', is always given, but often the frequency is not specified. In practice for many materials, the value of ε_r' is constant from DC up to around 5-10 GHz after which it begins to fall with frequency.

The value of σ is usually a strong function of frequency in the band of interest, increasing with frequency. This may be one reason why the imaginary part of the dielectric constant, or the loss tangent, is often specified in the literature: equations (12) and (16) show that these terms remove a linear frequency dependence compared to the frequency dependence of σ.

For each material a simple regression model for the frequency dependence of σ can be obtained by fitting to measured values of σ at a number of frequencies.

2.1.4 Models of material properties frequency dependence

In order to derive the frequency dependence of material properties, the values of the electrical constants of the materials can be characterized in terms of the measurement frequency, real part (ε_r') and imaginary part (ε_r'') of the relative permittivity, loss tangent (tan δ) and conductivity (σ). Note that the loss tangent can be derived from the conductivity and the imaginary part of the relative permittivity.

For the conductivity, there is usually statistically significant evidence for an increase with frequency. In this case the trend has been modelled using the simple formula:

$$\sigma = \alpha f^{\beta} \tag{28}$$

where f is the frequency in GHz. This is a straight line on a log(σ)–log(f) graph. The trend line is the best fit to all available data.

For the relative permittivity one can assume similar frequency dependency:

$$\varepsilon_r' = a\, f_{\mathrm{GHz}}^{b} \tag{29}$$

However in almost all cases there is no evidence of a trend of relative permittivity with frequency. In these cases a constant value can be used at all frequencies. The constant value is the mean of all the values plotted. Some examples are given in Table 4 of § 3.

2.2 Effects of material structure on radiowave propagation

2.2.1 Plane wave reflection and transmission at a single interface

2.2.1.1 Oblique incidence on dielectric media

The case of a sinusoidal plane wave incident obliquely to a plane interface separating two uniform dielectric media is considered. There are three important theorems for this case that follow from geometrical considerations.

1) The vector wave numbers of the reflected and transmitted (refracted) waves lie in the plane of incidence, i.e. the plane defined by wave number k_1 of the incident wave and the normal to the interface. This is taken to be the *x*-*z* plane in Fig. 3.

2) The angles of incidence and reflection are equal (both θ_1 in Fig. 3).

3) The angle of refraction, θ_2, is related to the angle of incidence by Snell's law.

$$\frac{1}{c_1}\sin\theta_1 = \frac{1}{c_2}\sin\theta_2 \tag{30}$$

where $c_1 = c/(\varepsilon_1\mu_1)^{1/2}$ and $c_2 = c/(\varepsilon_2\mu_2)^{1/2}$ are the respective wave speeds in the two media, ε_1 and ε_2 represent the complex relative permittivity of the two media, and μ_1 and μ_2 represent the relative permeability of the two media.

These theorems ensure that the exponential space-time factors, $\exp\{j(\omega t - k\cdot r)\}$, for the three waves ($k \rightarrow k_1, k_1', k_2$, respectively) are identical at all points in the interface.

FIGURE 3

Reflection and refraction of plane waves at plane interface

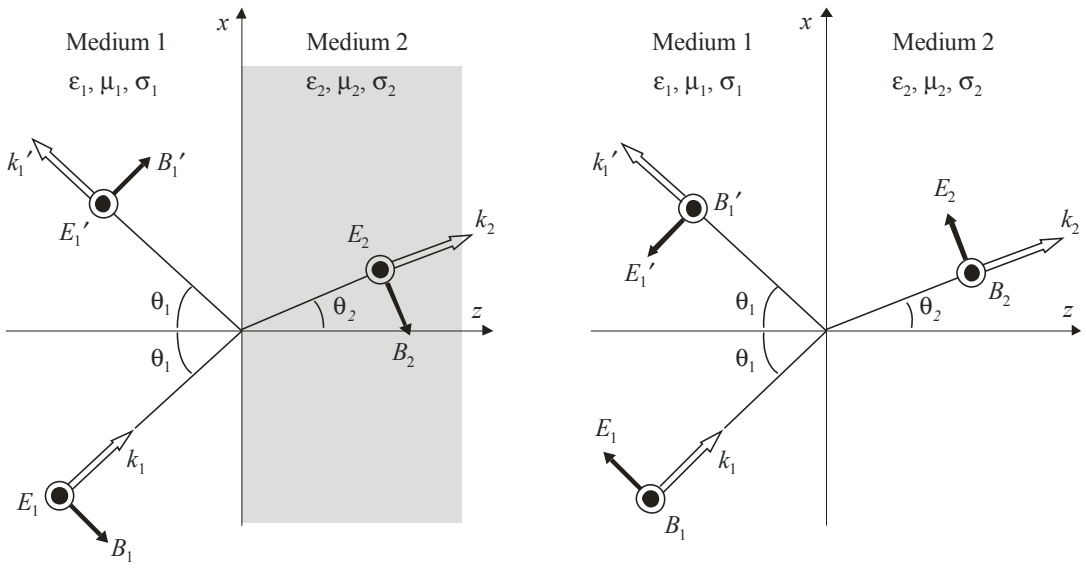

P.2040-03

The reflection and refraction coefficients are considered separately for the two cases below:

Case I – The incident electric field, E_1, is normal to the plane of incidence.

Case II – The incident electric field, E_1, is parallel to the plane of incidence.

Case I – (E-vector normal to the plane of incidence.)

The reflection and refraction coefficients, R_N and T_N, are derived as equations (31a) and (31b) based on the electromagnetic boundary condition.

$$R_N = \frac{-\mu_1 \tan\theta_1 + \mu_2 \tan\theta_2}{\mu_1 \tan\theta_1 + \mu_2 \tan\theta_2} \xrightarrow{\mu_1=\mu_2} -\frac{\sin(\theta_1 - \theta_2)}{\sin(\theta_1 + \theta_2)} \tag{31a}$$

$$T_N = \frac{2\mu_2 \tan\theta_2}{\mu_1 \tan\theta_1 + \mu_2 \tan\theta_2} \xrightarrow{\mu_1=\mu_2} \frac{2\cos\theta_1 \sin\theta_2}{\sin(\theta_1 + \theta_2)} \tag{31b}$$

The simplified forms shown for magnetically equivalent materials apply to the common special case of non-magnetic materials. In addition, angles θ_1 and θ_2 are not independent, being related by Snell's law as shown in equation (30). These coefficients can be represented as:

$$R_N = \frac{\mu_1 \eta_{12}^2 \cos\theta_1 - \mu_2 \sqrt{\eta_{12}^2 - \sin^2\theta_1}}{\mu_1 \eta_{12}^2 \cos\theta_1 + \mu_2 \sqrt{\eta_{12}^2 - \sin^2\theta_1}} \xrightarrow{\mu_1=\mu_2} \frac{\eta_{12}^2 \cos\theta_1 - \sqrt{\eta_{12}^2 - \sin^2\theta_1}}{\eta_{12}^2 \cos\theta_1 + \sqrt{\eta_{12}^2 - \sin^2\theta_1}} \tag{32a}$$

$$T_N = \frac{2\mu_2 \eta_{12} \cos\theta_1}{\mu_1 \eta_{12}^2 \cos\theta_1 + \mu_2 \sqrt{\eta_{12}^2 - \sin^2\theta_1}} \xrightarrow{\mu_1=\mu_2} \frac{2\eta_{12} \cos\theta_1}{\eta_{12}^2 \cos\theta_1 + \sqrt{\eta_{12}^2 - \sin^2\theta_1}} \tag{32b}$$

Case II − (E-vector parallel to the plane of incidence.)

The reflection and refraction coefficients for Case II, R_P and T_P, are similarly derived based on the electromagnetic boundary condition as:

$$R_P = \frac{-\varepsilon_1 \tan\theta_1 + \varepsilon_2 \tan\theta_2}{\varepsilon_1 \tan\theta_1 + \varepsilon_2 \tan\theta_2} \xrightarrow{\mu_1=\mu_2} \frac{\tan(\theta_1 - \theta_2)}{\tan(\theta_1 + \theta_2)} \tag{33a}$$

$$T_P = \frac{2\varepsilon_1 \sin\theta_1 / \cos\theta_2}{\varepsilon_1 \tan\theta_1 + \varepsilon_2 \tan\theta_2} \xrightarrow{\mu_1=\mu_2} \frac{2\cos\theta_1 \sin\theta_2}{\sin(\theta_1 + \theta_2)\cos(\theta_1 - \theta_2)} \tag{33b}$$

$$R_P = \frac{\mu_2 \cos\theta_1 - \mu_1 \sqrt{\eta_{12}^2 - \sin^2\theta_1}}{\mu_2 \cos\theta_1 + \mu_1 \sqrt{\eta_{12}^2 - \sin^2\theta_1}} \xrightarrow{\mu_1=\mu_2} \frac{\cos\theta_1 - \sqrt{\eta_{12}^2 - \sin^2\theta_1}}{\cos\theta_1 + \sqrt{\eta_{12}^2 - \sin^2\theta_1}} \tag{34a}$$

$$T_P = \frac{2\mu_2 \cos\theta_1}{\mu_2 \cos\theta_1 + \mu_1 \sqrt{\eta_{12}^2 - \sin^2\theta_1}} \xrightarrow{\mu_1=\mu_2} \frac{2\cos\theta_1}{\cos\theta_1 + \sqrt{\eta_{12}^2 - \sin^2\theta_1}} \tag{34b}$$

where η_{12} represents the relative complex permittivity of Medium 2 based on Medium 1.

$$\eta_{12} = \sqrt{\frac{\mu_2}{\mu_1}} \sqrt{\frac{\varepsilon_2 - j\sigma_2/\omega}{\varepsilon_1 - j\sigma_1/\omega}} \tag{35}$$

σ_1 and σ_2 represent the conductivity of the two media and ω is the angular frequency.

The formulas give the reflection and refraction coefficients for electromagnetic waves in a plane.

2.2.1.2 Normal incidence on a conductor

Consider the special case of a wave in vacuum (≈ air) impinging on a good conductor ($g >> \omega\varepsilon_0\kappa_e$) at normal incidence. Where, g is conductivity, ω is angle frequency, ε_0 is permittivity in vacuum, and κ_e is relative permittivity. As suggested in Fig. 4, the incident wave of amplitude E_1, travelling in the $+z$ direction, sets up the reflected wave of amplitude $\breve{E}_1'$ and the (damped) transmitted wave of initial amplitude $\breve{E}_2$.

When the conducting region is sufficiently thick, we may neglect a reflected wave approaching the interface from the right.

FIGURE 4

Reflection of a plane wave at the surface of a conductor (normal incidence)

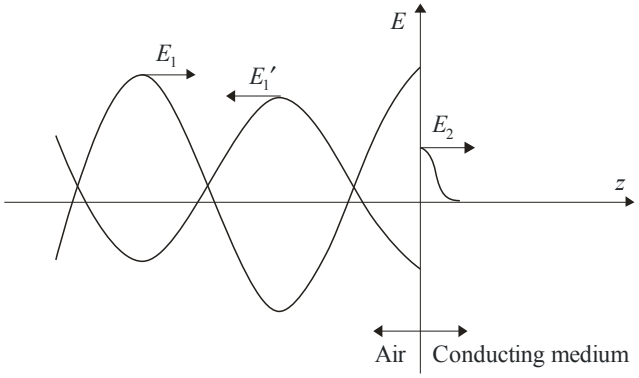

P.2040-04

The electric fields of the three linearly polarized, monochromatic, plane waves are expressed as follows:

Incident: $$E_1 e^{j(\omega t - \kappa_0 z)} \tag{36}$$

Reflected: $$E_1' e^{j(\omega t + \kappa_0 z)} \tag{37}$$

Transmitted: $$\breve{E}_2 e^{-\frac{z}{\delta_e} j\left(\omega t - \frac{z}{\delta}\right)} \tag{38}$$

where $\kappa_0 = \omega/c$ is the vacuum wave number, δ is the skin-depth parameter of the conductor and expressed as follows:

$$\delta = \left(\frac{2}{\omega\mu_0\kappa_m g}\right)^{\frac{1}{2}} \tag{39}$$

where, μ_0 is permeability in vacuum, κ_m is relative permeability of the medium. The plane-wave fields are transverse; hence only tangential components exist at the boundary plane ($z = 0$). The cups on the symbols $\breve{E}_1'$ and $\breve{E}_2$ signify that the amplitudes are complex quantities, i.e. that the

reflected and transmitted waves may not be in phase with the incident wave of prescribed amplitude and phase.

The magnetic fields of the three waves are expressed as follows;

Incident: $$B_1 e^{j(\omega t-\kappa_0 z)}=\frac{E_1}{c}e^{j(\omega t-\kappa_0 z)} \tag{40}$$

Reflected: $$\breve{B}'_1 e^{j(\omega t+\kappa_0 z)}=\frac{\breve{E}'_1}{c}e^{j(\omega t+\kappa_0 z)} \tag{41}$$

Transmitted: $$\breve{B}_2 e^{-\frac{z}{\delta}j\left(\omega t-\frac{z}{\delta}\right)}\approx(1-j)\frac{\breve{E}_2}{\omega\delta}e^{-\frac{z}{\delta}j\left(\omega t-\frac{z}{\delta}\right)} \tag{42}$$

Again, the magnetic vectors lie in the same plane, perpendicular to that of the electric vectors, and are tangential to the boundary.

The following equations for the tangential components are derived from the boundary conditions at $z = 0$.

$$E_1+\breve{E}'_1=\breve{E}_2 \tag{43}$$

$$E_1-\breve{E}'_1=(1-j)\frac{c}{\omega\delta\kappa_m}\breve{E}_2 \tag{44}$$

These yield the (complex) reflection and transmission coefficients for the electric field amplitudes as follows:

$$\breve{R}_E\equiv\frac{\breve{E}'_1}{E_1}=\frac{-(1-j)\left(\frac{c}{\omega\delta\kappa_m}\right)+1}{(1-j)\left(\frac{c}{\omega\delta\kappa_m}\right)+1}\approx-\left[1-(1+j)\frac{\omega\delta\kappa_m}{c}\right] \tag{45}$$

$$\breve{T}_E\equiv\frac{\breve{E}_2}{E_1}=\frac{2}{(1-j)\left(\frac{c}{\omega\delta\kappa_m}\right)+1}\approx(1+j)\frac{\omega\delta\kappa_m}{c} \tag{46}$$

The power reflection coefficient is simply as follows:

$$R_p=\left|\breve{R}_E\right|^2=\frac{1+\left(1-\frac{\omega\delta\kappa_m}{c}\right)^2}{1+\left(1+\frac{\omega\delta\kappa_m}{c}\right)^2}\approx1-\frac{2\omega\delta\kappa_m}{c} \tag{47}$$

Conservation of energy requires that the power transmission coefficient, i.e. the fraction of the incident power dissipated in the conductor is expressed as follows:

$$T_p = 1 - R_p = \frac{\frac{4\omega\delta\kappa_m}{c}}{1 + \left(1 + \frac{\omega\delta\kappa_m}{c}\right)^2} \approx \frac{2\omega\delta\kappa_m}{c} \tag{48}$$

For a good conductor ($g \to \infty$, $\delta \to 0$), the wave is almost perfectly reflected.

2.2.2 Plane wave reflection and transmission through single and multilayer slabs

2.2.2.1 Single slab

2.2.2.1.1 Method

If we assume that the building material is a homogeneous dielectric single-layer plate with a smooth surface, with the geometry shown in Fig. 5, we can express the transmission coefficient, T, of the building material as:

$$T = \frac{\left(1 - R'^2\right)\exp\left(-j\left(\delta - k_0 d\right)\right)}{1 - R'^2 \exp\left(-j2\delta\right)} \quad \text{(transmission coefficient)} \tag{49}$$

where:

$$\delta = 2\pi d / \lambda \cdot \sqrt{\eta - \sin^2\theta}$$

$$k_0 = 2\pi / \lambda$$

d : thickness of the building material

λ : wavelength in free space

η : complex permittivity

θ : angle between the incident ray and the plane of the surface normal to the reflecting surface ($0 \le \theta \le 90°$) (Fig. 5).

In equation (49), R' is given by R_N or R_P,

R_N (E-vector normal to the reflection plane) (50)

R_P (E-vector parallel to the reflection plane) (51)

where R_N and R_P are Fresnel's reflection coefficients for the interface between air and a dielectric medium when the electric field is perpendicular and parallel to the incident plane, respectively.

2.2.2.1.2 Calculation results

The transmission loss of a dielectric wall of a building is calculated for concrete with complex permitivities provided by Recommendation ITU-R P.1238, § 7. The results are presented in Fig. 6. In this figure, the vertical axis and horizontal axis show the transmission loss in dB and the thickness of the wall normalized by the wavelength in free space (d/λ), respectively. The results of $\theta = 0°$, $30°$, and $60°$ are plotted.

FIGURE 5

Transmission geometry

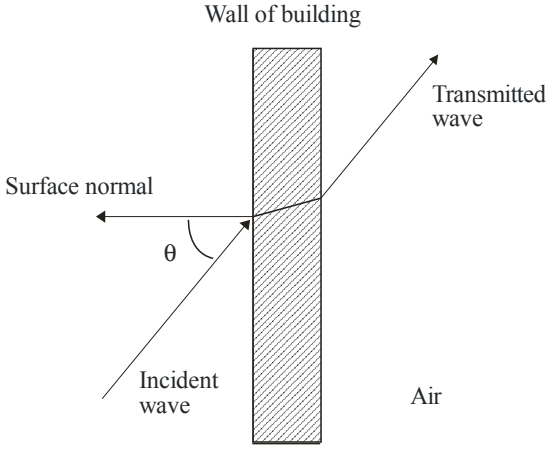

FIGURE 6

Calculated transmission loss of single-layer concrete wall in case of TE incidence
Concrete material with complex permittivity = η = 7.0 – *j*0.85 at 1 GHz

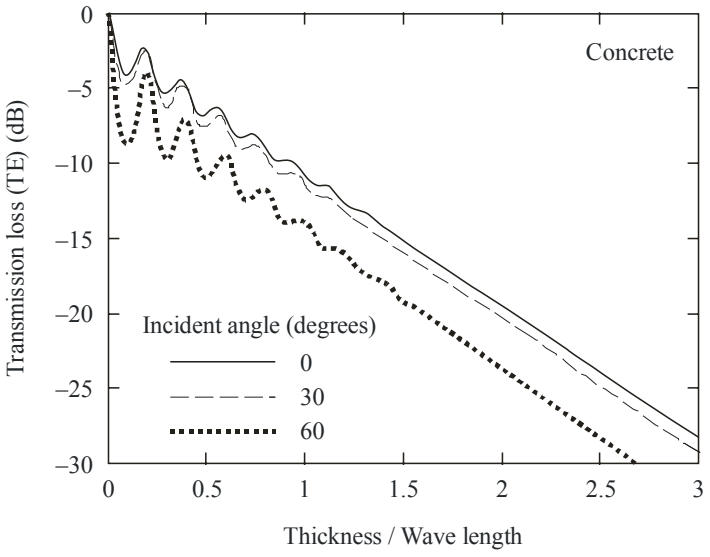

2.2.2.2 Multilayer slabs

If we assume that the building material is a homogeneous dielectric multi-layer slab with a smooth surface, the reflection and transmission characteristics can be evaluated by the reflection and transmission coefficients based on Recommendation ITU-R P.1238, which are defined by:

$$R_N = \frac{E_N^r}{E_N^i} \tag{52a}$$

$$R_P = \frac{E_P^r}{E_P^i} \tag{52b}$$

$$T_N = \frac{E_N^t}{E_N^i} \tag{52c}$$

$$T_P = \frac{E_P^t}{E_P^i} \tag{52d}$$

where E represents the complex amplitude of the E-fields and the superscripts i, r, and t denote incident, reflected, and transmitted E-fields, respectively. The subscripts N and P denote the E-field components normal or parallel to the reflection plane, respectively, where the reflection plane is the plane in which both the incident and reflected rays lie (see Fig. 7 for the geometry). The incident and reflected E-fields are defined at the reflecting surface while the transmitted E-field is defined at the surface opposite to the reflecting surface. The reference directions for E_P and E_N, and the direction of propagation always form a local right-handed orthogonal coordinate in this order. The reference directions of E_N for incident, reflected, and transmitted E-fields are defined to be identical.

FIGURE 7

Geometry for calculating reflection characteristics

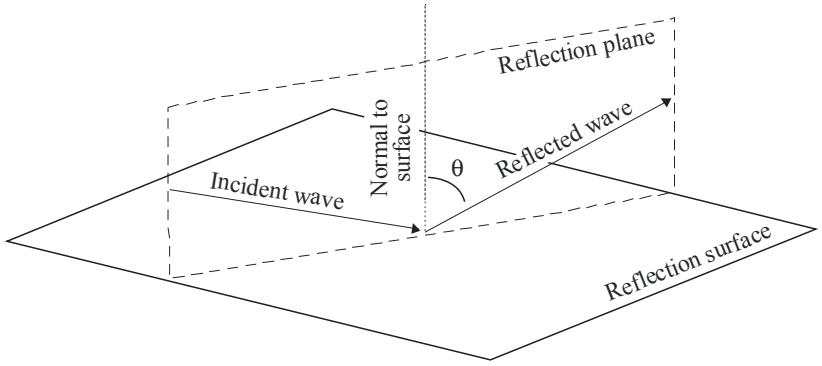

P.2040-07

From complex permittivity η, the reflection coefficient is given by:

$$R_N = \frac{\cos\theta - \sqrt{\eta - \sin^2\theta}}{\cos\theta + \sqrt{\eta - \sin^2\theta}} \quad (E - \textit{field component normal to the reflection plane}) \tag{53a}$$

$$R_P = \frac{\cos\theta - \sqrt{\eta - \sin^2\theta/\eta^2}}{\cos\theta + \sqrt{\eta - \sin^2\theta/\eta^2}} \quad (E - \textit{field component parallel to the reflection plane}) \tag{53b}$$

where θ is the angle between the incident ray and the normal to the reflecting surface as shown in Fig. 7.

For the special case when the incident E-field is circularly polarized, changes in the amplitude and phase of the received signal from the reflected E-field can be represented by reflection coefficient R_C for circular polarization given by:

$$R_C = \frac{R_N + R_P}{2} \quad \text{(Circular polarization)} \tag{53c}$$

The above formulas are applicable when the penetration loss of the building material is large so that no significant wave is reflected back to the reflecting surface. When this is not the case, the effect of multiple internal reflections inside the building material must be taken into account.

When the building material is represented by N dielectric slabs, and the thickness and the complex permittivity of the m-th layer (m = 1, 2, … N) are given as d_m and η_m, respectively, the reflection and transmission coefficients are given by:

$$R_N = \frac{B_0}{A_0} \tag{54a}$$

$$R_P = \frac{G_0}{F_0} \tag{54b}$$

$$T_N = \frac{1}{A_0} \tag{54c}$$

$$T_P = \frac{1}{F_0} \tag{54d}$$

Here A_0, B_0, F_0, and G_0 are determined from the recursion formulas as:

$$A_m = \frac{\exp(\delta_m)}{2}\left[A_{m+1}(1+Y_{m+1}) + B_{m+1}(1-Y_{m+1})\right] \tag{55a}$$

$$B_m = \frac{\exp(-\delta_m)}{2}\left[A_{m+1}(1-Y_{m+1}) + B_{m+1}(1+Y_{m+1})\right] \tag{55b}$$

$$F_m = \frac{\exp(\delta_m)}{2}\left[F_{m+1}(1+W_{m+1}) + G_{m+1}(1-W_{m+1})\right] \tag{55c}$$

$$G_m = \frac{\exp(-\delta_m)}{2}\left[F_{m+1}(1-W_{m+1}) + G_{m+1}(1+W_{m+1})\right] \tag{55d}$$

$$A_{N+1} = 1 \tag{56a}$$

$$B_{N+1} = 0 \tag{56b}$$

$$F_{N+1} = 1 \tag{56c}$$

$$G_{N+1} = 0 \tag{56d}$$

$$W_{m+1} = \frac{\cos\theta_{m+1}}{\cos\theta_m}\sqrt{\frac{\eta_m}{\eta_{m+1}}} \tag{57a}$$

$$Y_{m+1} = \frac{\cos\theta_{m+1}}{\cos\theta_m}\sqrt{\frac{\eta_{m+1}}{\eta_m}} \tag{57b}$$

$$\eta_0 = \eta_{N+1} = 1 \tag{57c}$$

$$\delta_m = jk_m d_m \cos\theta_m \tag{58a}$$

$$k_m = \frac{2\pi}{\lambda}\sqrt{\eta_m} \tag{58b}$$

$$k_0 = k_{N+1} = \frac{2\pi}{\lambda} \tag{58c}$$

where:

λ : wavelength in free space

θ_m : angle of refraction in the m-th layer

θ_{N+1} : angle of refraction in air to the right of the last plane boundary.

Appendix 1 provides a method for calculating reflection and transmission characteristics for multi-layered materials by using the ABCD matrix formulation as an alternative computational method.

2.2.2.3 Total internal reflection

The angle of refraction θ_2, is related to the angle of incidence θ_1, by Snell's law as stated in equation (30)

$$\frac{1}{c_1}\sin\theta_1 = \frac{1}{c_2}\sin\theta_2 \tag{59}$$

where c_1 and c_2 are the respective wave speeds in the two media as shown in Fig. 3.

Substituting the index of refractions $n_1 = c/c_1$ and $n_2 = c/c_2$ to equation (59) will result in:

$$\frac{n_1}{n_2}\sin\theta_1 = \sin\theta_2 \tag{60}$$

If $n_1 > n_2$, then $\sin\theta_1 < \sin\theta_2$. This implies that $\sin\theta_2$ will reach the maximum value of 1 before $\sin\theta_1$. The maximum value that θ_1 can have is then limited to:

$$\sin\theta_c = \frac{n_2}{n_1} \tag{61}$$

where θ_c is called the critical angle of incidence.

When the angle of incidence exceeds the critical angle of incidence, the incident wave is completely reflected; this state is referred to as "total internal reflection".

2.2.2.4 Divergence and focusing of waves

The total electric field of the incident and reflected wave in medium 1 of Fig. 3 is considered. For Case I, consider the special case of free space in medium 1 and perfect conductor in medium 2, where the electric field component is normal to the plane of incidence as shown in Fig. 3.

The electric field of the incident wave and reflected wave can be expressed as follows:

$$\text{Incident: } E_y^{\,i} = E_1 e^{-jk_o(x\sin\theta_1 + z\cos\theta_1)} \tag{62}$$

$$\text{Reflected: } E_y^{\,r} = \breve{E}_1' e^{-jk_o(x\sin\theta_1 - z\cos\theta_1)} \tag{63}$$

where k_0 is the vacuum wave number.

The reflection coefficient of a perfect conductor is –1, therefore

$$\breve{E}_1' = -E_1 \tag{64}$$

The total electric field of the incident wave and reflected wave in free space can then be expressed as:

$$E = E_y^{\,i} + E_y^{\,r} = E_1 e^{-jk_o(x\sin\theta_1 + z\cos\theta_1)} - E_1 e^{-jk_o(x\sin\theta_1 - z\cos\theta_1)} \tag{65}$$

$$E = -2jE_1 \sin(k_o z\cos\theta_1) e^{-jk_o x\sin\theta_1} \tag{66}$$

In medium 1, when the x value is kept constant, the variation of the electric field at the z axis results in the divergence and focusing of wave independent of time. This wave is called a standing wave, and is a result of the interference between the incident and reflected wave. To illustrate this effect, the magnitude of the total electric field for $E_1 = 1$, $k_0 = 30$, $x = 0$, and incident angle = 10º is plotted in Fig. 8.

FIGURE 8

Magnitude of total electric field for Case I of medium 1

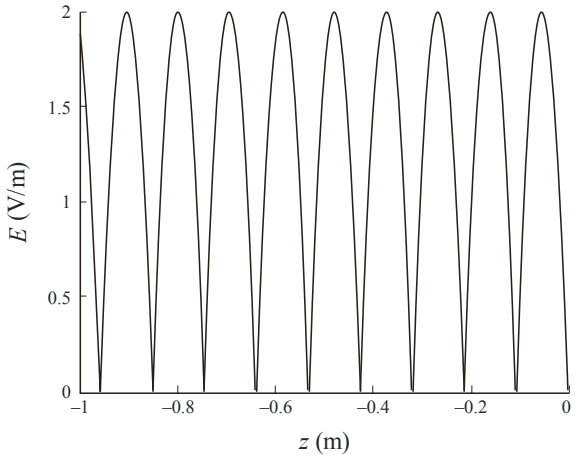

P.2040-08

2.2.3 Effects of non-uniform structures

2.2.3.1 Scattering from periodic objects (regular structures)

When a plane electromagnetic wave incidents a periodic structure, as shown in Fig. 9, and passes through the apertures, the power of the waves from the periodic apertures is maximized under condition (67) and is minimized under condition (68).

$$d(\sin\theta + \sin\varphi) = n\lambda \text{ and} \tag{67}$$

$$d(\sin\theta + \sin\varphi) = \left(n + \frac{1}{2}\right)\lambda \tag{68}$$

where:

d : distance between apertures

θ : angle of incident

φ : angle of departure

λ : wavelength

n : an integer.

FIGURE 9

Scattering from periodic objects

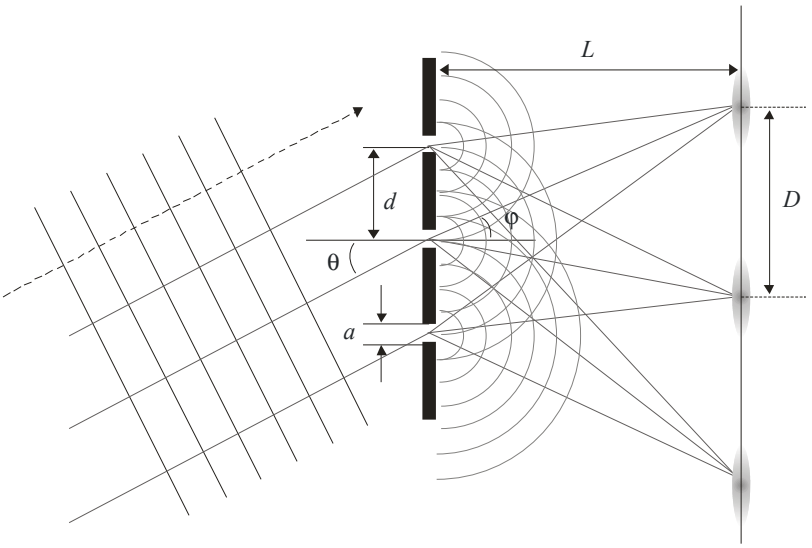

P.2040-09

The cycle of maxima can be estimates using equation (69) under the condition $L >> d$.

$$D = \frac{\lambda L}{d} \tag{69}$$

Under the condition $\theta = 0$, the intensity of wave I can derived by:

$$I = \frac{I_0}{m^2} \frac{\sin^2\left(\frac{\pi a}{\lambda}\sin\varphi\right)\sin^2\left(\frac{\pi d}{\lambda}\sin\varphi\right)}{\left(\frac{\pi a}{\lambda}\sin\varphi\right)^2\left(\frac{\pi d}{\lambda}\sin\varphi\right)^2} \tag{70}$$

where:

I_0 : intensity at $\theta = 0$

m : number of apertures

a : aperture width.

2.2.3.2 Electromagnetic plane wave penetration through apertures and structures

2.2.3.2.1 UTD simulation and measurement results

2.2.3.2.1.1 Introduction

A window in a building wall can usually be treated as an aperture, because the penetration loss through a glass window is generally smaller than that through surrounding surface walls made from other materials such as stone, brick and concrete.

There are many empirical or theoretical methods for evaluating the influence of the aperture on building entry loss. The examples below are evaluated using the geometrical optics (GO) approach.

A three-dimensional (3D) box with an open aperture is defined, and calculations results given for different aperture sizes. These calculations are compared with measurement.

2.2.3.2.1.2 Method

The assumed model is given in Fig. 10. Angle θ is the angle between the incident ray and the plane normal to the aperture ($0 \leq \theta \leq 90°$). Figure 11 shows the geometrical model for evaluating the influence of the aperture on the building entry loss. A three dimensional (3D) model is assumed. The top and bottom of Fig. 11 are the floor plan and the elevation diagram, respectively.

FIGURE 10

Assumed model

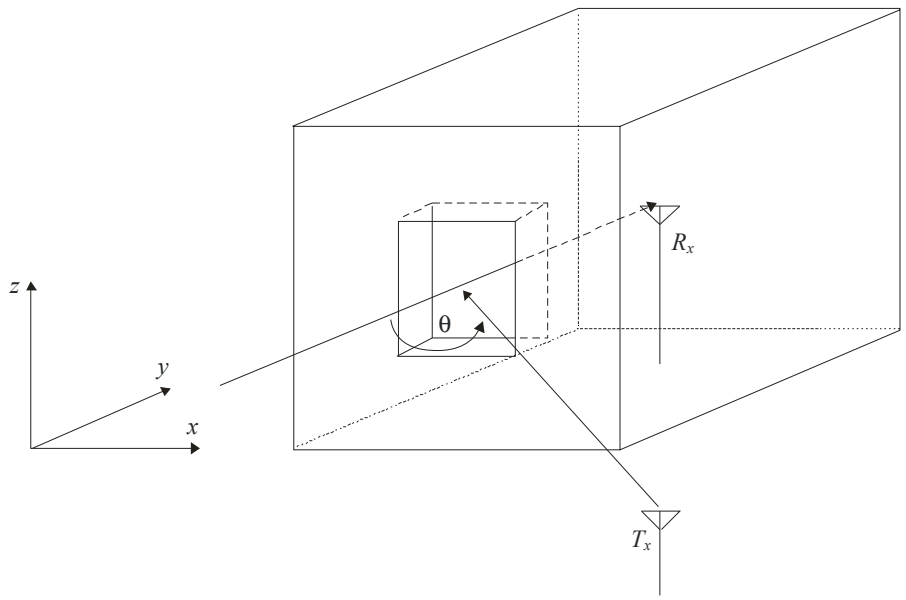

P.2040-10

FIGURE 11

Geometrical model for evaluating the influence of the aperture on the building entry loss

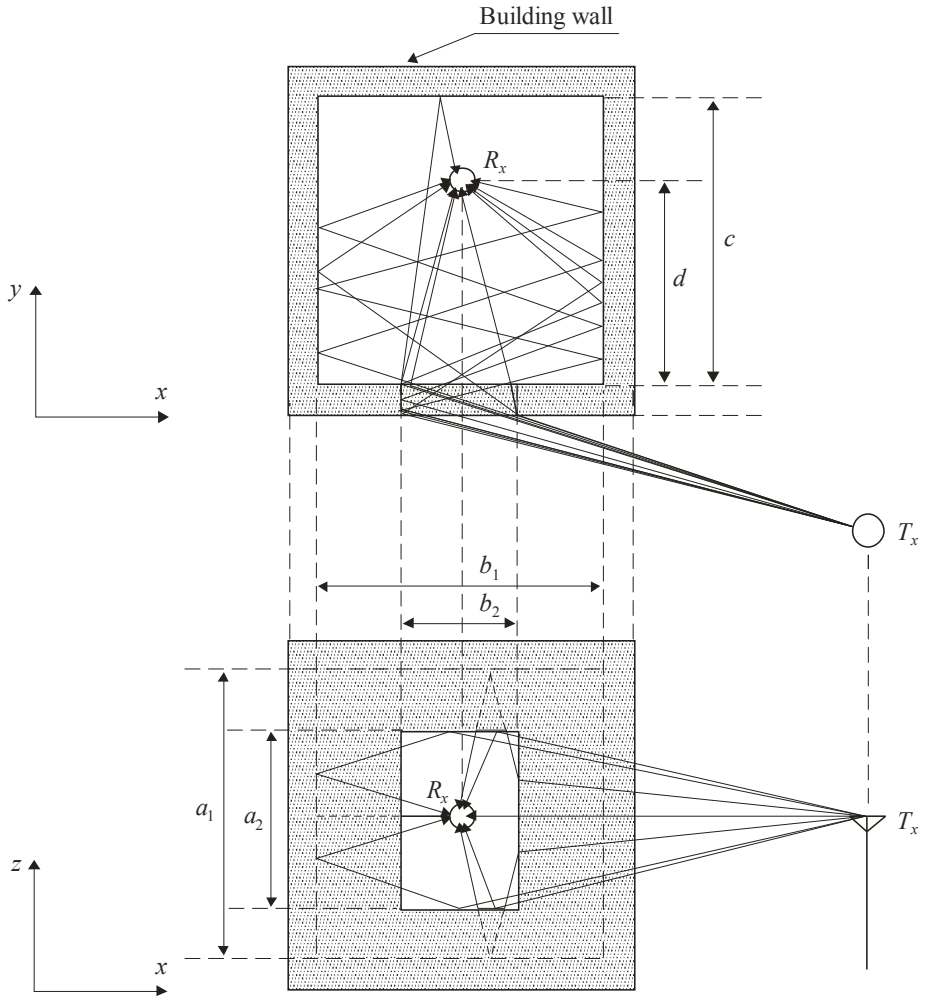

Top: floor plan

Bottom: elevation

P.2040-11

The parameters given in Fig. 11 are given below.

d : distance of receiver R_x from the aperture of the building

T : thickness of the building wall (all walls are assumed the same)

a_1 : vertical size of the room

a_2 : vertical size of the aperture

b_1 : horizontal size of the room

b_2 : horizontal size of the aperture

c : depth of the room from the aperture.

It was assumed that the aperture was set at the centre of the building wall.

The following waves are considered in the analysis:

1) Direct wave (line-of-sight (LoS) region).
2) 1-4 times reflected waves from any surface.
3) Diffracted waves from the wedges of the aperture.
4) Diffracted-reflected waves from the wedge of the aperture and the wall of the room.
5) Reflected-diffracted waves from the wall of the room and the wedge of the aperture.

2.2.3.2.1.3 Calculation results

Two cases, A and B, are considered. The difference between the two cases is the size of the aperture. The dimensions of the aperture and room are shown in Table 1. The frequency is 5 GHz. Vertical polarization is considered. The material and complex permittivity of the building walls are assumed to be concrete and 7.0-*j*0.85, respectively. The reflection and diffraction coefficients used in the 3D geometrical optics are the Fresnel reflection coefficient and UTD diffraction coefficient, respectively. The angle θ is 40°. The reception antenna (Rx) is moving along a straight line that is through the centre of the aperture and parallel with y-axis in Fig. 11. The transmission antenna height is the same as the reception antenna height.

The result is shown in Fig. 12. In these figures, the vertical axis and horizontal axis represent the excess loss from the free-space loss at d = 0 m and the distance from the aperture, d, respectively. The results of Cases A and B are plotted.

TABLE 1

Dimensions used in calculation

	Case A	**Case B**
d (Moving distance from the aperture) (m)	0-3 (5-cm step)	0-3 (5-cm step)
T (cm)	5	5
a_1 (m)	2.32	2.32
a_2 (m)	2.32	1.3
b_1 (m)	2.64	2.64
b_2 (m)	2.64	1.3s
c (m)	3.6	3.6
θ (°)	50	50
Area of aperture (m^2)	6.12	1.69

2.2.3.2.1.4 Measurement

The measurements of the building entry loss were carried out in a general apartment. The geometry of the measurements is similar to that in Figs 10 and 11. The room and aperture dimensions are similar to those given in Table 1. However, the assumed aperture type for the measurements is only used in Case B. Angle θ is 50°. The frequency is 5.2 GHz. The Tx and Rx antennas are a directional antenna whose beam width in the horizontal plane is 60° and an omnidirectional antenna, respectively. The polarization is vertical. The measurement results are presented in Fig. 12 with the calculated results for both Cases A and B. Although the calculated results for Case B seem to overestimate the excess loss in the midrange of "*d*" by comparison with the measured results, the calculated results for Case B is in good agreement with the measured results in terms of the tendency. That is, the entry loss becomes small as "*d*" becomes large in the NLoS region. Of

course, these phenomena strongly depend on many factors such as the room dimensions or the location of the Rx antenna; nevertheless, we can recognize the mechanisms of the influence of the aperture on the building entry loss.

FIGURE 12

Building entry loss at 5.2 GHz
Frequency, polarization, and θ are 5.2 GHz, Vertical, and 50°, respectively

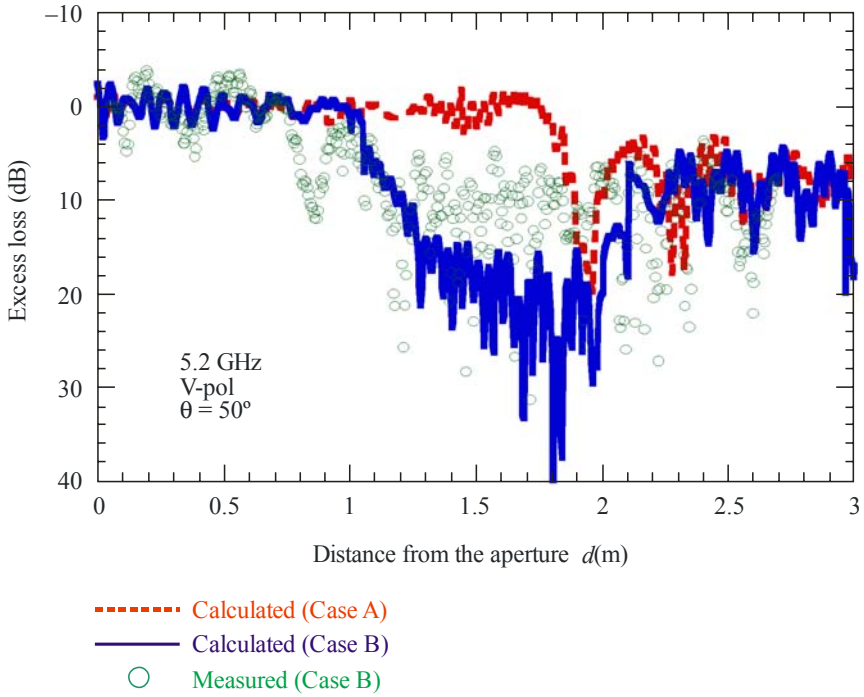

P.2040-12

2.2.3.2.2 The uniform geometrical theory of diffraction (UTD) for a wedge obstacle

2.2.3.2.2.1 Method

The uniform geometrical theory of diffraction can be used to predict the diffraction loss due to a finitely conducting wedge. Suitable applications are for diffraction around the corner of a building or over the ridge of a roof, or where terrain can be characterized by a wedge-shaped hill. The method requires the conductivity and relative dielectric constant of the obstructing wedge, and assumes that no transmission occurs through the wedge material.

The method for computing the diffraction loss due a finitely conducting wedge is given in Recommendation ITU-R P.526. It takes account of diffraction in both the shadow and LoS region, and a method is provided for a smooth transition between these regions.

2.2.3.2.2.2 Comparison of measured and calculated results

The simple measurements of the diffraction loss against a conducting wedge of 90º were carried out in an anechoic chamber. The geometry of the measurement setup is shown in Fig. 13. The transmitting antenna, Tx was fixed and the receiving antenna, Rx was moved to shadow region from lit region. The frequency was 5.2 GHz, and both vertical and horizontal polarization cases were tested. The measured results are shown in Fig. 14 with the calculated results using UTD.

FIGURE 13

Geometry of measurement

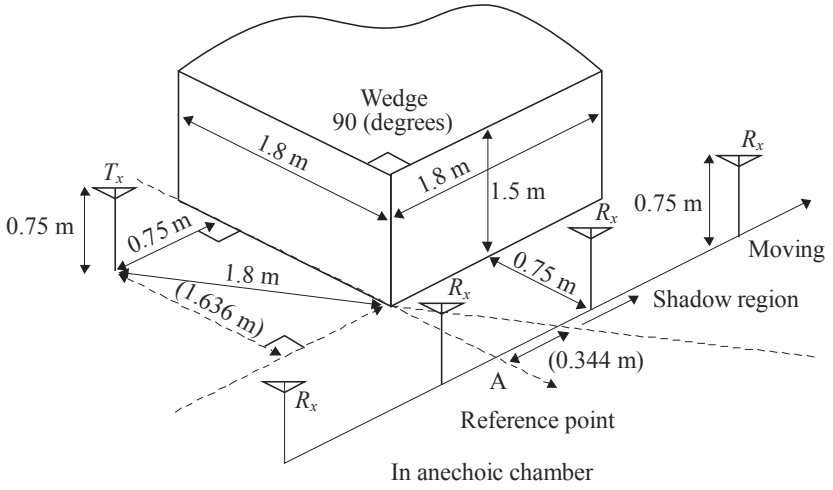

P.2040-13

FIGURE 14

Measured and calculated results for diffraction loss of conducting wedge

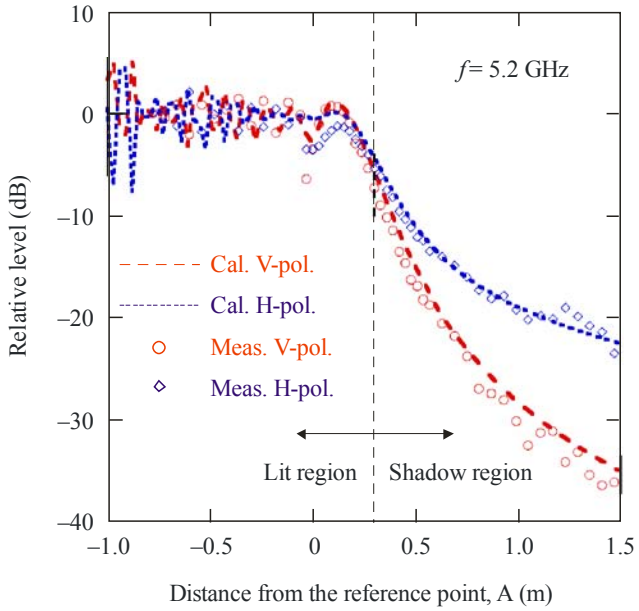

P.2040-14

The measured results are in very good agreement with the calculated results using UTD when both vertical and horizontal polarization cases are considered.

2.2.3.2.3 Electromagnetic equivalence principle

The electromagnetic equivalence principle is used to estimate an electromagnetic field, and the concept is illustrated in Fig. 15.

Electric and magnetic fields are respectively radiated by an electric current and magnetic current within virtual boundary *S*. Here, the electric field and magnetic field inside virtual boundary *S* are

respectively represented by $\vec{E}_i$ and $\vec{H}_i$, and electric field $\vec{E}_0$ and magnetic field $\vec{H}_0$ outside of virtual boundary $\vec{S}$ are represented by $\vec{E}_0$ and $\vec{H}_0$, respectively.

FIGURE 15

Equivalent electromagnetic current

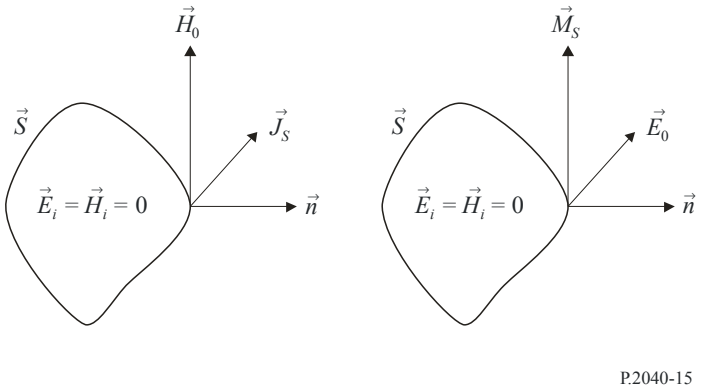

a) Magnetic field and the equivalent electric current

b) Electric field and the equivalent magnetic current

From the boundary condition, electric field and magnetic field must be continuously at the virtual boundary $\vec{S}$. The following equations are given.

$$\begin{aligned} &\vec{n}\times(\vec{H}_0 - \vec{H}_i) = 0 \\ &-\vec{n}\times(\vec{E}_0 - \vec{E}_i) = 0 \end{aligned} \tag{71}$$

Here, from the vector product of the electric and magnetic currents at boundary $\vec{S}$ and the normal vector for boundary $\vec{S}$, equivalent electric current $\vec{J}_s$ and equivalent magnetic current $\vec{M}_s$ can be expressed as:

$$\begin{aligned} &\vec{J}_s = \vec{n}\times\vec{H}_0 \\ &\vec{M}_s = -\vec{n}\times\vec{E}_0 \end{aligned} \tag{72}$$

Therefore, without information regarding the original electromagnetic source, the electromagnetic field outside the boundary can be estimated from the information regarding the electromagnetic field at the boundary.

2.2.3.2.4 Babinet's principle

Babinet's principle states that the diffraction patterns of two complementary screens as shown in Fig. 16, i.e. one has apertures where the other is opaque, and vice versa, are such that the vector sum of the respective diffracted amplitudes, ψ_1 and ψ_2 (not intensities) at any point is equal to the amplitude of the original wave when no screen is present, ψ_0. Thus, if the diffraction pattern of a certain aperture is known, the pattern of the corresponding obstacle can be obtained readily.

FIGURE 16

Babinet's principle

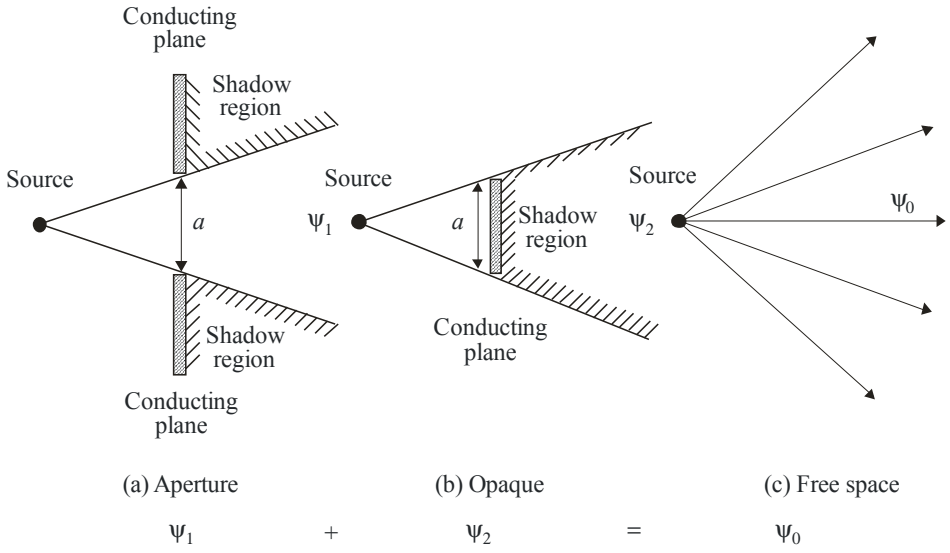

2.2.3.3 Waveguides and resonant cavities

2.2.3.3.1 Theory on frequency characteristics of attenuation constant in waveguide

A waveguide may comprise of a hollow space surrounded by lossy dielectric materials. In the case of a building structure, a corridor, underground mall, or tunnel can be considered as a waveguide. The radiowave power that propagates in a waveguide is attenuated according to the distance. It is well known that a waveguide has frequency characteristics such as the cut-off frequency that varies according to the shape. In this section, a formula is presented to derive the attenuation constant for the frequency characteristics in a waveguide.

The cross-section of a square waveguide structure is shown in Fig. 17. In this case, the intrinsic constants of the lossy dielectric material are different for the sidewalls and for the ceiling and the floor.

FIGURE 17

Cross-section of waveguide and material constants

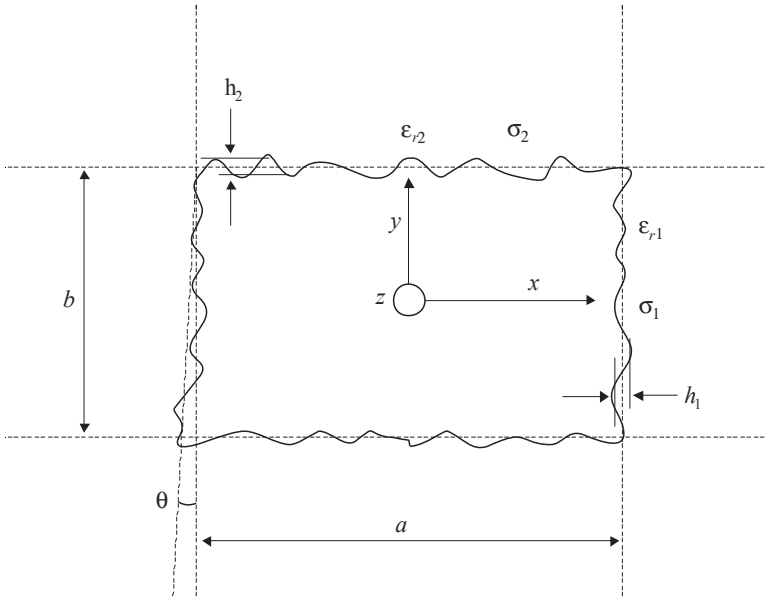

In Fig. 17, ***a*** is the width and ***b*** is the height of the waveguide (m), h_1 and h_2 are the root mean square roughness of the Gaussian distribution of the surface level, and θ is the tilt of the root mean square (rad). The complex permittivity values for materials ε_{ri}^{*} are calculated as follows.

$$\varepsilon_{ri}^{*} = \varepsilon_{ri} - j\left(\varepsilon_{ri}'' + \frac{\sigma_i}{\varpi\varepsilon_0}\right), \qquad i = 1,2 \tag{73}$$

where ε_{ri} is the relative dielectric constant and σ_i is the conductivity. The quantity ε_{ri}'' is the loss tangent of the materials, ω is the angular frequency and ε_0 is the permittivity of free space.

The basic attenuation constant is formulated as follows.

$$L_{basic,h} = \mathrm{K_h}\lambda^2\left[\mathrm{Re}\left(\frac{\varepsilon_{r1}^{*}}{a^3\sqrt{\varepsilon_{r1}^{*}-1}} + \frac{1}{b^3\sqrt{\varepsilon_{r2}^{*}-1}}\right) - \frac{\lambda}{2\pi}\mathrm{Im}\left(\frac{\left|\varepsilon_{r1}^{*}\right|^2}{a^4\left(\varepsilon_{r1}^{*}-1\right)} + \frac{1}{b^4\left(\varepsilon_{r2}^{*}-1\right)}\right)\right]$$

$$L_{basic,v} = \mathrm{K_v}\lambda^2\left[\mathrm{Re}\left(\frac{1}{a^3\sqrt{\varepsilon_{r1}^{*}-1}} + \frac{\varepsilon_{r2}^{*}}{b^3\sqrt{\varepsilon_{r2}^{*}-1}}\right) - \frac{\lambda}{2\pi}\mathrm{Im}\left(\frac{1}{a^4\left(\varepsilon_{r1}^{*}-1\right)} + \frac{\left|\varepsilon_{r2}^{*}\right|^2}{b^4\left(\varepsilon_{r2}^{*}-1\right)}\right)\right] \quad \text{(dB/m)} \tag{74}$$

$\mathrm{K_h}$ and $\mathrm{K_v}$ are constant values that are dependent on the section shape. The constant values dependent on the section shape are given in Table 2.

TABLE 2

Constant values for various cross-section shapes

Shape	Circle	Ellipse	Square	Arch-backed
K_h	5.09	4.45	4.34	5.13
K_v	5.09	4.40	4.34	5.09

The formulas mentioned above are valid based on equation (75) representing the condition of constraint.

$$\lambda << \frac{\pi a \sqrt{\varepsilon_{r1} - 1}}{\varepsilon_{r1}} \quad \text{(m)} \qquad (75)$$
$$\lambda << \pi b \sqrt{\varepsilon_{r2} - 1}$$

Unique characteristics in square shape case

The attenuation constant due to roughness, which is regarded as local variations in the level of the surface relative to the mean level of the surface of a wall, is formulated in equation (76).

$$L_{roughness,h} = K_h \pi^2 \lambda \left[\left(\frac{h_1}{a^2} \right)^2 + \left(\frac{h_2}{b^2} \right)^2 \right]$$
$$L_{roughness,v} = K_v \pi^2 \lambda \left[\left(\frac{h_1}{a^2} \right)^2 + \left(\frac{h_2}{b^2} \right)^2 \right] \quad \text{(dB/m)} \qquad (76)$$

The attenuation constant due to the wall tilt is formulated in equation (77).

$$L_{tilt,h} = K_h \frac{\pi^2 \theta^2}{\lambda}$$
$$L_{tilt,v} = K_v \frac{\pi^2 \theta^2}{\lambda} \quad \text{(dB/m)} \qquad (77)$$

Therefore, the total attenuation constant in a square shape case is the sum of the above losses as follows.

$$L_h = L_{basic,h} + L_{roughness,h} + L_{tilt,h}$$
$$L_v = L_{basic,v} + L_{roughness,v} + L_{tilt,v} \quad \text{(dB/m)} \qquad (78)$$

2.2.3.3.2 Applicability of waveguide theory

The waveguide theory shows good agreement with the measured propagation characteristics in the corridor in the frequency range of 200 MHz to 12 GHz in case there is no pedestrian traffic in the corridor.

Effect of pedestrian traffic on waveguide

Figure 18 shows a comparison of the theoretical and measured attenuation constant values during the day (when pedestrian traffic is present), and during the night (when the corridor is empty). Theoretical values are calculated based on the parameters given in Table 3.

TABLE 3

Parameters used in underground calculation

	Width (m)	Height (m)	Tilt (degrees)	Roughness		Material constant			
				h_1	h_2	ε_{r1}	ε_{r2}	σ_1	σ_2
Underground	6.4	3.0	0.35	0.4	0.2	15	10	0.5	0.1

FIGURE 18

Attenuation constant comparison for day and night

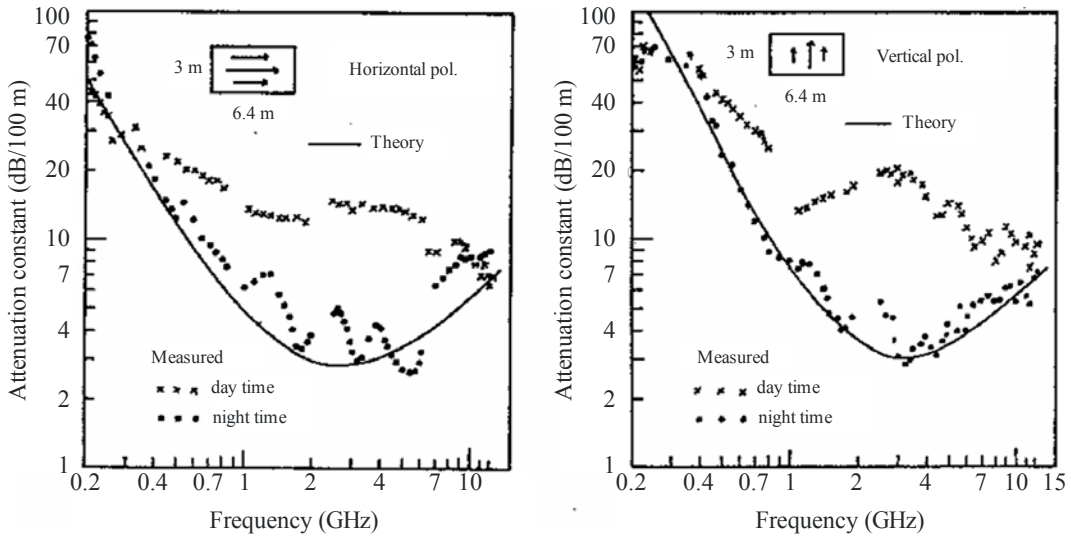

P.2040-18

Figure 18 shows that the waveguide theory is applicable to realistic propagation characteristics in the corridor in the frequency range of 200 MHz to 12 GHz at night. However, the waveguide theory is not applicable to realistic propagation characteristics during daytime, because the received power is attenuated by pedestrian traffic.

Therefore the waveguide theory is applicable to situations where there is no influence from shadowing obstacles.

2.3 Theory and results for frequency selective surface materials

2.3.1 Frequency selective surfaces

The power of scattering waves varies with roughness of surfaces. In this section, a theory for calculating scattered fields from the surface having round convexity array is described. First, for parameterizing the roughness of the surface, the rough surface is defined by using a round convexity array formed by locating circular cylinders periodically. Second, the reflection coefficient of the scattered fields is defined by using the lattice sums characterizing a periodic arrangement of scatterers and the T-matrix for a circular cylinder array. Third, a numerical result that shows the

frequency-depending characteristic of the reflection from the round convexity's surface is shown. Finally, a measurement result is shown to explain that the power of scattering waves varies with the frequency of an incident wave when there is a round convexity array on the surface of a building.

2.3.2 Theory for wave propagation around the surface of round convexity array

By making periodical round convexity array on a surface of a building, as shown in Fig. 19, reflection/scattering waves can be controlled larger than those from the flat surface. The theory to calculate the scattered waves from the periodic arrays of circular cylinders can be used to define the propagation waves around a convexity array of a surface.

FIGURE 19

The surface of round convexity array

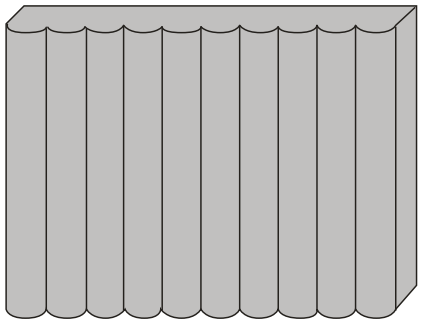

P.2040-19

FIGURE 20

Geometry of a periodic array of circular cylinders

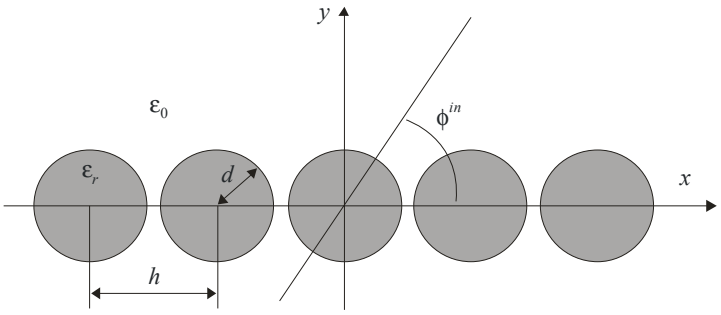

P.2040-20

When the identical circular cylinders are situated periodically in an x axis as shown in Fig. 20, the power reflection coefficient R_ν for the ν-th propagating mode with $k_\nu > 0$ is given as:

$$R_\nu = \frac{k_\nu}{\mathrm{k_0 \sin \varphi^{in}}} |\boldsymbol{p}_\nu^T \cdot \boldsymbol{a}_0^{\mathrm{sc}}|^2 \tag{79}$$

where $k_0 = 2\pi / \lambda_0$, λ_0 is the wavelength of the waves indenting in angle φ^{in}. In equation (79), $\boldsymbol{p}_\nu^T$ and $\boldsymbol{a}_0^{\mathrm{sc}}$ are obtained as follows:

$$\boldsymbol{p}_\nu = \begin{bmatrix} \frac{2(j)^m (k_{x\nu} + jk_\nu)^m}{hk_\nu k_0^m} & (m \geq 0) \\ \frac{2(-j)^{|m|} (k_{x\nu} - jk_\nu)^{|m|}}{hk_\nu k_0^{|m|}} & (m < 0) \end{bmatrix} \tag{80}$$

$$\boldsymbol{a}_0^{\mathrm{sc}} = (\bar{\boldsymbol{I}} - \bar{\boldsymbol{T}} \cdot \bar{\boldsymbol{L}})^{-1} \cdot \bar{\boldsymbol{T}} \cdot \boldsymbol{a}^{in} \tag{81}$$

where $\bar{\boldsymbol{I}}$ is the unit matrix, $k_{xv} = -k_0 \cos\varphi^{in} + 2v\pi/h$, $k_v = \sqrt{k_0^2 - k_{xv}^2}$ and h is the periodic space between each round convex. $\bar{\boldsymbol{L}}$ is a square matrix whose elements are defined in terms of the following lattice sums:

$$L_{mn} = \sum_{l=0}^{\infty} H_{m-n}^{(1)}(k_0 lh) e^{jk_0 lh\varphi^{in}} + (-1)^{m-n} \sum_{l=0}^{\infty} H_{m-n}^{(1)}(k_0 lh) e^{-jk_0 lh\varphi^{in}} \tag{82}$$

where $H_m^{(2)}$is the m-th order Hankel function of the first kind. $\bar{\boldsymbol{T}}$ is the T-matrix for the scattered fields and is given by the following diagonal matrix for the incident electric field E_z^{in} and the incident magnetic field H_z^{in}, respectively.

$$T_{mn}^{E} = -\frac{\sqrt{\varepsilon_r} J_m'(kd) J_m(k_0 d) - J_m(kd) J_m'(k_0 d)}{\sqrt{\varepsilon_r} J_m'(kd) H_m^{(1)}(k_0 d) - J_m(kd) H_m'^{(1)}(k_0 d)} \delta_{mn} \tag{83}$$

$$T_{mn}^{\mathrm{H}} = -\frac{J_m'(kd) J_m(k_0 d) - \sqrt{\varepsilon_r} J_m(kd) J_m'(k_0 d)}{J_m'(kd) H_m^{(1)}(k_0 d) - \sqrt{\varepsilon_r} J_m(kd) H_m'^{(1)}(k_0 d)} \delta_{mn} \tag{84}$$

where ε_r is the relative permittivity of the dielectric cylinder, J_m is the m-th order Bessel function, the prime demotes the derivative with respect to the argument, and δ_{mn} denotes the Kronecker's delta. $\boldsymbol{a}^{in}$ denotes a column vector whose elements represent unknown amplitudes of the incident field.

$$\boldsymbol{a}^{in} = \left[(j)^n e^{-jn\varphi^{in}}\right] \tag{85}$$

2.3.3 Calculation results

The calculation result of a power reflection coefficient is shown in Fig. 21. The result is calculated by using equation (79) in the case that the electric field E_z^{in} is transmitted in the angle φ^{in}=90° to the dielectric round convexities whose diameter and permittivity are d=0.3h and ε_r=2.0, respectively. In the result, there is the frequency band that the incident wave is reflected almost completely by the surface even if its material is a lossless dielectric substance.

FIGURE 21

Power reflection coefficient R_0 as functions of the normalized wavelength h/λ_0 at normal incidence electric field E_z^{in}

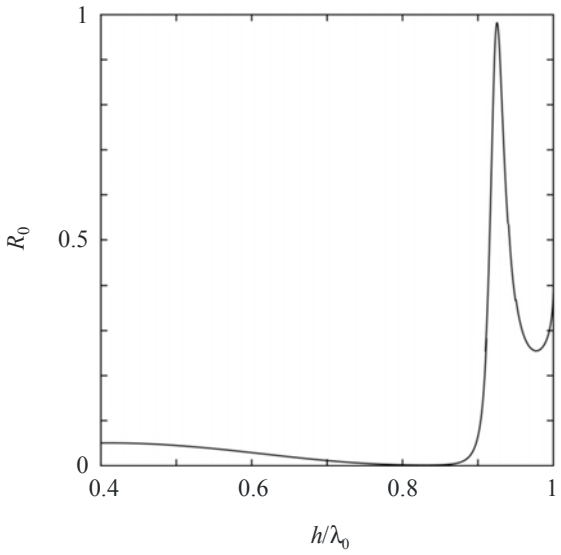

P.2040-21

2.3.4 Measurement

The measurements of the scattered waves from the building having the round convexity array were carried out. Figure 22 shows the comparison of the scattered waves from the building between the flat surface and the surface with round convexity arrays. The scattered waves from the building were measured in various reflected angles φ^r between 30° to 90°, when the electric field is transmitted in the angle φ^{in}. The incident angle and reflection angle are defined as shown in Fig. 23.

FIGURE 22

Geometry of a periodic array of circular cylinders

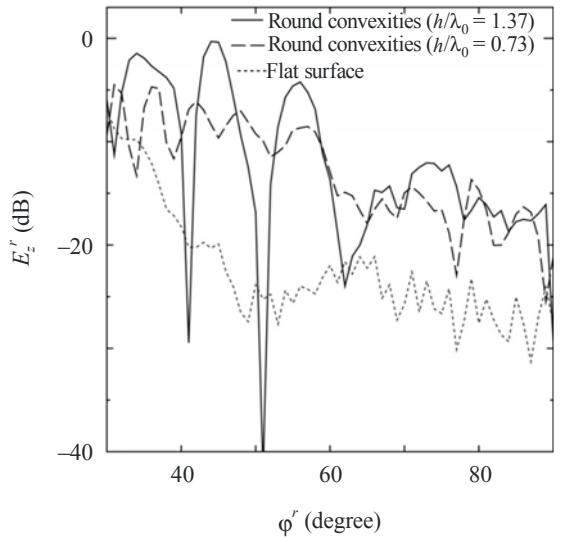

P.2040-22

FIGURE 23

A plane figure of the compositional diagram for measurements

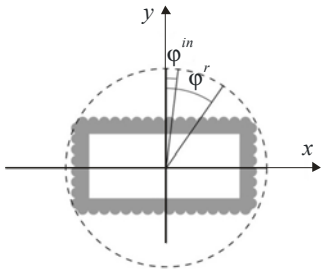

P.2040-23

The measurement results show that the power of the scattered field from the surface having a round convexity array becomes larger than that from the flat surface, and can be controlled by the period between and diameter of each round convexity. Note that the relative permittivity and the conductivity of the building material were estimated as $\varepsilon_r = 6.0$ and $\sigma = 0.1$ S/m, respectively.

3 Compilations of electrical properties of materials

Representative data on material electrical properties can be hard to find, as characteristics are expressed using different combination of parameters, and the relative permittivity may be quoted at frequencies that are not close to that of interest. A table of representative material properties has therefore been compiled using the curve-fitting approach described in § 2.1.4.

Data from eight sets of material electrical properties (a total of more than 90 separate characteristics) given in the open literature have been collated, converted to a standard format and grouped into material categories. For each group, simple expressions for the frequency dependence of the relative permittivity, ε_r', and the conductivity, σ, were derived. These are:

$$\varepsilon_r' = a\, f_{\mathrm{GHz}}^{b} \tag{86}$$

and:

$$\sigma = c\, f_{\mathrm{GHz}}^{d} \ \mathrm{S/m} \tag{87}$$

where f_{GHz} is the frequency in GHz and σ is in S/m. (ε_r' is dimensionless.) The values of a, b, c and d are given in Table 4. Where the value of b or d is absent, this indicates that the value of ε_r' or σ is constant (with value a or c) independent of frequency. This is equivalent to setting the value of b or d to zero.

If required, the imaginary part of the relative permittivity ε_r'' can be obtained from the conductivity and frequency:

$$\varepsilon_r'' = 17.98\,\sigma / f \tag{88}$$

TABLE 4

Material properties

Material class	Relative permittivity		Conductivity		Frequency range
	a	*b*	*c*	*d*	GHz
Concrete	5.31	0	0.0326	0.8095	1-100
Brick	3.75	0	0.038	0	1-10
Plasterboard	2.94	0	0.0116	0.7076	1-100
Wood	1.99	0	0.0047	1.0718	0.001-100
Glass	6.27	0	0.0043	1.1925	0.1-100
Ceiling board	1.50	0	0.0005	1.1634	1-100
Chipboard	2.58	0	0.0217	0.7800	1-100
Floorboard	3.66	0	0.0044	1.3515	50-100
Metal	1	0	10^7	0	1-100
Very dry ground	3	0	0.00015	2.52	1-10 only
Medium dry ground	15	−0.1	0.035	1.63	1-10 only
Wet ground	30	−0.4	0.15	1.30	1-10 only

The frequency limits given in Table 4 are not hard limits but are indicative of the frequency limits of the data that were used to derive the models. The exceptions are the three ground types where the 1-10 GHz frequency limits must not be exceeded. Typical values of relative permittivity and conductivity for different types of ground, as function of frequency in the range 0.01 MHz to 100 GHz are given in Recommendation ITU-R P.527.

The loss tangents of all the dielectric materials in Table 4 are less than 0.5 over the frequency ranges specified. The dielectric limit approximations for the attenuation rate given in equations (24) and (27) can therefore be used to estimate the attenuation of an electromagnetic wave through the materials:

$$A_{dielectric} = 1636 \frac{\sigma}{\varepsilon_r'} \text{ dB/m} \tag{89}$$

where ε_r' and σ are given by equations (86) and (87).

4 Building loss measurements

4.1 Building entry loss

4.1.1 Building entry loss measurements (Europe)

Measurements have been carried out in Germany and the United Kingdom to determine values of building entry loss and other parameters to be used in planning indoor reception of broadcasting services.

The German measurements were made at two frequencies in the VHF band used for digital audio broadcasting and two frequencies in the UHF band. The median values of the building entry loss over all measurements made in buildings typical for Germany were 9.1 dB at 220 MHz, 8.5 dB at 223 MHz, 7.0 dB at 588 MHz and 8.5 dB at 756 MHz.

The penetration loss from the front of the building (the side with higher signal level) into a room on the opposite side has median values of 14.8 dB at 220 MHz, 13.3 dB at 223 MHz, 17.8 dB at 588 MHz and 16 dB at 756 MHz.

Over all measurements, the median values of the location variation standard deviations are 3.5 dB for the 220 and 223 MHz signals with 1.5 MHz bandwidth and 5.5 dB for the 588 and 756 MHz signals with 120 kHz bandwidth.

The United Kingdom measurements were made at a number of frequencies in the UHF band.

The median building entry loss at UHF was found to be 8.1 dB with a standard deviation of 4.7 dB. However, the value for rooms on the side of the building furthest from the transmitter was 10.3 dB, whereas the corresponding value for rooms on the side of the building nearest to the transmitter was 5.4 dB; a difference of about 5 dB.

A median value of 13.5 dB was measured for the outdoors height gain between 1.5 and 10 m. The locations of the measurements were suburban.

The median value of the difference in field strength between ground floor and first floor rooms was found to be 5.4 dB.

The standard deviation of the variation of field strength within rooms was about 3 dB.

The standard deviation of the variation of field strength measured for a floor of a house was about 4 dB.

Despite differences in the frequencies and bandwidths of the measurements, there is very good agreement between the German and United Kingdom measurements.

4.1.2 Building entry loss measurements (Japan)

Entry loss measurements were made in Japan on 12 office buildings at distances from the transmitter of up to 1 km.

The additional path loss to points within a building was measured relative to the outdoor field averaged along a path around the building at 1.5 m height. Note that the use of the fixed height reference differs from the definition of building entry loss given in § 1.2, and will lead to negative values of entry loss for higher floors of the building.

The data from these measurements has been fitted by the following expression for excess path loss with respect to the averaged 1.5 m value:

$$\Delta Loss\,(\mathrm{dB}) = 0.41 \cdot d - 0.5 \cdot h - 2.1 \cdot \log(f) - 0.8 \cdot LoS + 11.5 \tag{90}$$

where:

d: 0 to 20 m; the distance from the window (m)

h: 1.5 to 30 m; the height from the ground (m)

f: 0.8 to 8 GHz; the frequency (GHz)

LoS: 1 for line-of-sight, LoS = 0 for non-line-of-sight.

4.1.3 Building entry loss – slant path measurements

4.1.3.1 UHF satellite signal measurements (860 MHz-2.6 GHz)

Representative UHF satellite signal attenuation observed within rooms located near an exterior wall in timber-framed private homes is summarized in Table 5. For interior rooms, 0.6 dB must be added to the tabulated values. For timber-framed buildings the attenuation shows little variation with

weather or path elevation angle but, as the Table illustrates, there is a systematic variation with frequency, polarization, construction materials, insulation and position within the structure. Some aluminium-backed insulating and construction materials contribute up to 20 dB of loss.

TABLE 5

UHF signal attenuation (dB) through timber-framed buildings*

Building condition		Frequency (MHz) and polarization (Horizontal: H, Vertical: V)			
Exterior	Insulation (non-metallic type)	860 H	860 V	1 550 V	2 569 V
Wood siding	Ceiling only	4.7	2.9	5.0	5.8
	Ceiling and wall	6.3	4.5	6.6	7.4
Brick veneer	Ceiling only	5.9	4.1	6.2	7.0
Bricks	Ceiling and wall	7.5	5.7	7.8	8.6

* The Table is for rooms located near to the exterior wall; for interior rooms, 0.6 dB should be added.

4.1.3.2 Slant-path measurements from towers or high rise buildings

Measurements of building entry loss using 18 to 20 m towers to simulate a satellite transmitter were performed in the bands 700 MHz to 1.8 GHz and 500 MHz to 3 GHz to determine the mean loss and spatial variability in a variety of buildings. There are insufficient data to give precise prediction methods, but the data in Tables 6 to 7 are indicative.

TABLE 6

Signal distributions at the average position and best position within buildings (over the frequency range 700 to 1 800 MHz)

Building number	Construction	Elevation angle	Average position		Best position	
			Mean loss (dB)	Standard deviation (dB)	Mean loss (dB)	Standard deviation (dB)
1	Corner office, large windows, single-story building. Concrete block, plasterboard, double-glazing. Concrete roof on steel beams	27.5° (LoS through window, azimuth angle between wall and LoS is 50°)	7.9	5.5	4.2	4.2
2	Small room with windows being 5/8 of exterior wall	18° (LoS through window, azimuth angle between wall and LoS is 50°)	9.1	4.4	5.4	3.7

TABLE 6 (*end*)

Building number	Construction	Elevation angle	Average position		Best position	
			Mean loss (dB)	Standard deviation (dB)	Mean loss (dB)	Standard deviation (dB)
3	Corner foyer, large reflective glass door in half of one exterior wall. External walls concrete, internal walls plasterboard on metal frame	16° (LoS through window, 45° azimuth angle between one wall and LoS, both exterior walls illuminated by transmitter)	15.4	8.4	9.7	6.7
4	Sheet metal shack with plywood interior. One small unscreened window on each of two sides, metal-covered door	25° (azimuth angle between wall and LoS is 60°)	9.7	6.3	5.2	4.9
5	Two-story wood-side house, rockwool insulation (walls and attic); gypsum board, no metallic heat-shield. No metallic screens on windows. Wood-shingled roof	25° (azimuth angle between wall and LoS is 45°)	9.0	4.5	5.4	3.7
6	Empty sheet-metal mobile trailer home, metal frame windows with metal screens	25° (azimuth angle between wall and LoS is 45°)	24.9	3.8	19.8	3.4

TABLE 7

Median loss at the average position and best position within buildings as a function of frequency (Construction details and elevation angle as in Table 9)

Building number	Average position	Best position
(As in Table 6)	750-1 750 MHz	750-1 750 MHz
1	5-11 dB	2-6 dB
2	5-14 dB	2-5 dB
3	17-18 dB	12-13 dB
4	9-11 dB	5-6 dB
5	5-11 dB	3-5 dB
6	20 to > 24 dB	16-22 dB

TABLE 8

Signal distributions at the average position within buildings (estimated over the frequency range 500-3 000 MHz)

Building number	Construction	Elevation angle (degrees)	Average position	
			Mean loss (dB)	Standard deviation (dB)
1	Entry lobby in single storey building – concrete tilt wall, tar roof	18	13	10
2	Office in single storey building – block brick, tar roof	38	9	7
3	Two-storey wood frame farmhouse, metal roof, no aluminium heat-shield	33	5	4
4	Hallway and living room of two-storey woodframe house, metal roof, aluminium heat-shield	41	19.5	12
5	Motel room in two-storey building, brick with composite roof	37	13	6
6	Lobby of two-storey building, glass and concrete, tar roof	26	12	5

In the first set of measurements (Tables 6 and 7), the first three buildings had elevation angles such that the room was illuminated through a window with a direct LoS from the transmitter. The elevation angles were below 30° to allow side illumination of the buildings.

In the case of building number 3 in these tables, losses through the reflective glass door were about 15 dB greater than when the door was open.

The results of another study are similar, with mean attenuation levels (in the frequency range 500 to 3 000 MHz) varying between 5 dB for a woodframe house with metal roof and no aluminium heat-shield, to 20 dB for a similar house with an aluminium heat-shield. Table 11 shows a summary of the measured mean attenuation values.

Note that for some of the measurements, values obtained near a window or an open door, are included in the averaging. In the motel (building 6), attenuation when the direct path penetrated a brick wall was 15 to 30 dB below the LoS value. Levels inside building 4 varied from 25 to 45 dB below the LoS value, due to the metal roof and aluminium heat-shield.

Note also that the measurements were on stationary paths. There is evidence that close-in multipath effects will give rise to fluctuations in received signal level should the transmitter or receiver move. This has implications particularly for low-Earth orbit (LEO) systems where the transmitter is moving rapidly with respect to the receiver.

The measurements indicate that attenuation increases with frequency by about 1 to 3 dB/GHz in buildings 1, 2, 4, and 6, by 6 dB/GHz in the least attenuating building (building 3), and shows almost no change with frequency in the glass-walled building 5. Since the values given above are averaged over the frequency range 500 MHz to 3 GHz, they are expected to be slightly optimistic for the 1 to 3 GHz range.

For the six buildings identified in Table 8, 1.6 GHz and 2.5 GHz measurements were performed and analysed to determine the median, 5% and 95% levels of relative signal loss when the antennas were moved horizontally over multiple 80 cm intervals. The buildings were illuminated from the

side, and the signals received inside the outside wall (one-wall entry). Azimuthally omnidirectional antennas were used to receive the transmitted signals. Statistics derived from these measurements are summarized in Fig. 24. These data indicate the magnitude and variations of fading that are possible for signal transmission through building walls. Note that on occasions, multipath conditions yield relative signal levels in excess of 0 dB.

FIGURE 24

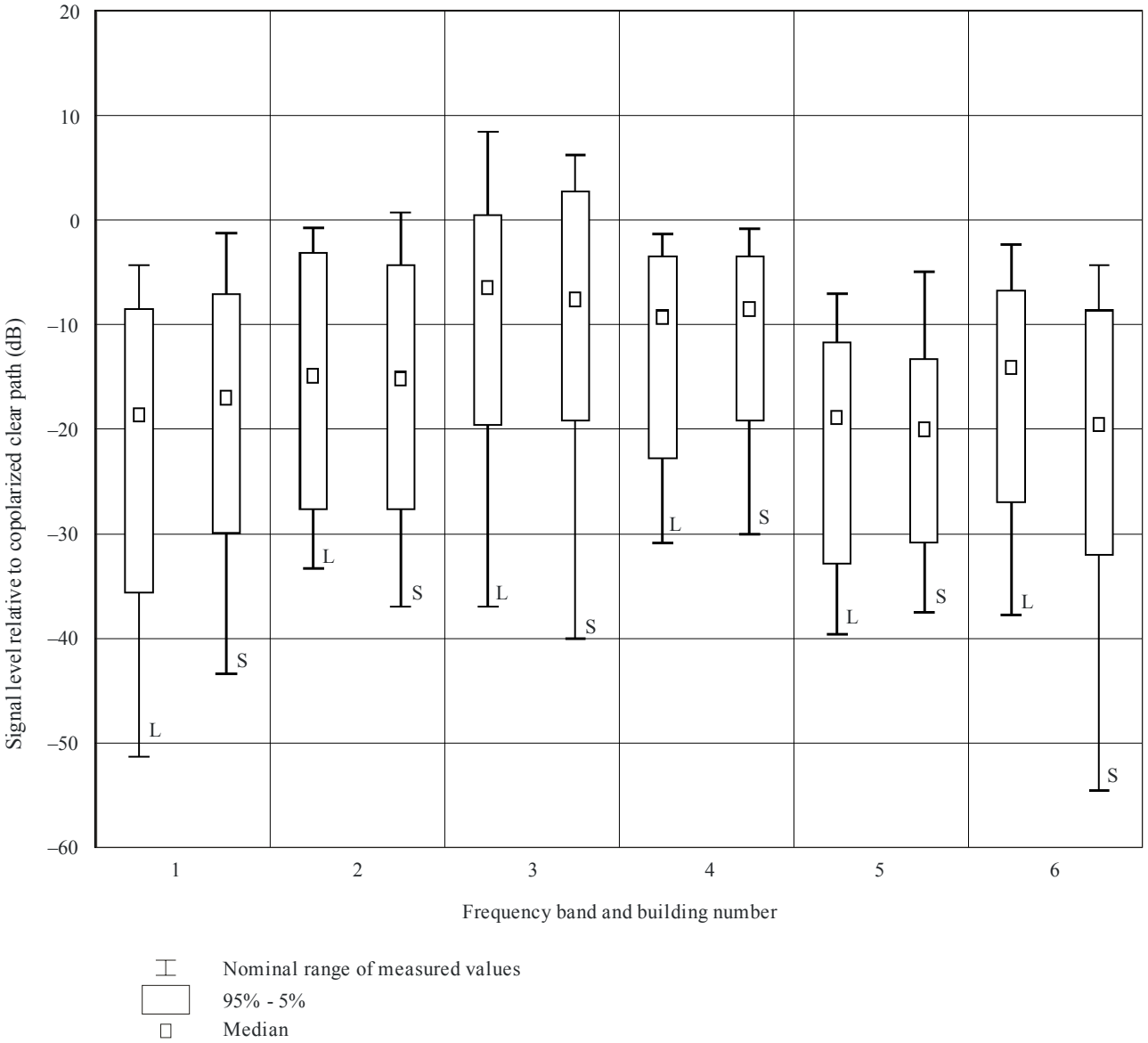

Median, 5% and 95% levels of building entry power loss relative to unobstructed LoS at 1.6 GHz and 2.5 GHz for the six buildings identified in Table 5 (designated by 1 to 6 in the Figure). For each building, the 1.6 GHz (L) and 2.5 GHz (S) statistics are shown separately.

P.2040-24

None of the available measurements at frequency bands below 3 GHz provides information for elevation angles above 41°. However, the large losses through metal structures (building 6 in Tables 6 and 7; building 4 in Table 8) suggest that attenuation for a direct path through a metal roof will be of the order of 20 dB. The losses of 15 to 30 dB for a brick wall in building 4 of Table 8 are relevant for higher elevation angles as well.

The elevation angle dependence of building entry loss was measured in the 5 GHz band at two different elevation angles by using high-rise buildings to simulate the reception of satellite signals. In an office-type room, the measured medians of the excess building entry loss were 20 dB and 35 dB for elevation angles of 15° and 55°, respectively.

4.1.3.3 Helicopter measurements to office building

The elevation and azimuth angle dependencies of building entry loss around 5 GHz were measured at different positions within an eight-storey building on three different floors. A helicopter was used to simulate a satellite transmitter. The received signal was continuously recorded, as well as the position of the helicopter by means of a differential global positioning system (GPS) receiver. The experimental conditions and averaged measurement results are summarized in Table 9. The behaviour of the building entry loss with respect to path elevation angle is shown in Fig. 25, and the behaviour with respect to azimuth in Fig. 26 for elevation angles of 15° and 30°.

FIGURE 25

Building entry loss at 5.1 GHz at sections 1, 2 and 3 for floors 2, 5 and 6. The angle Ψ_E is positive-defined when looking to the north and negative-defined to the south $|\Psi_E| = 90° - \varepsilon$ where ε is the elevation angle

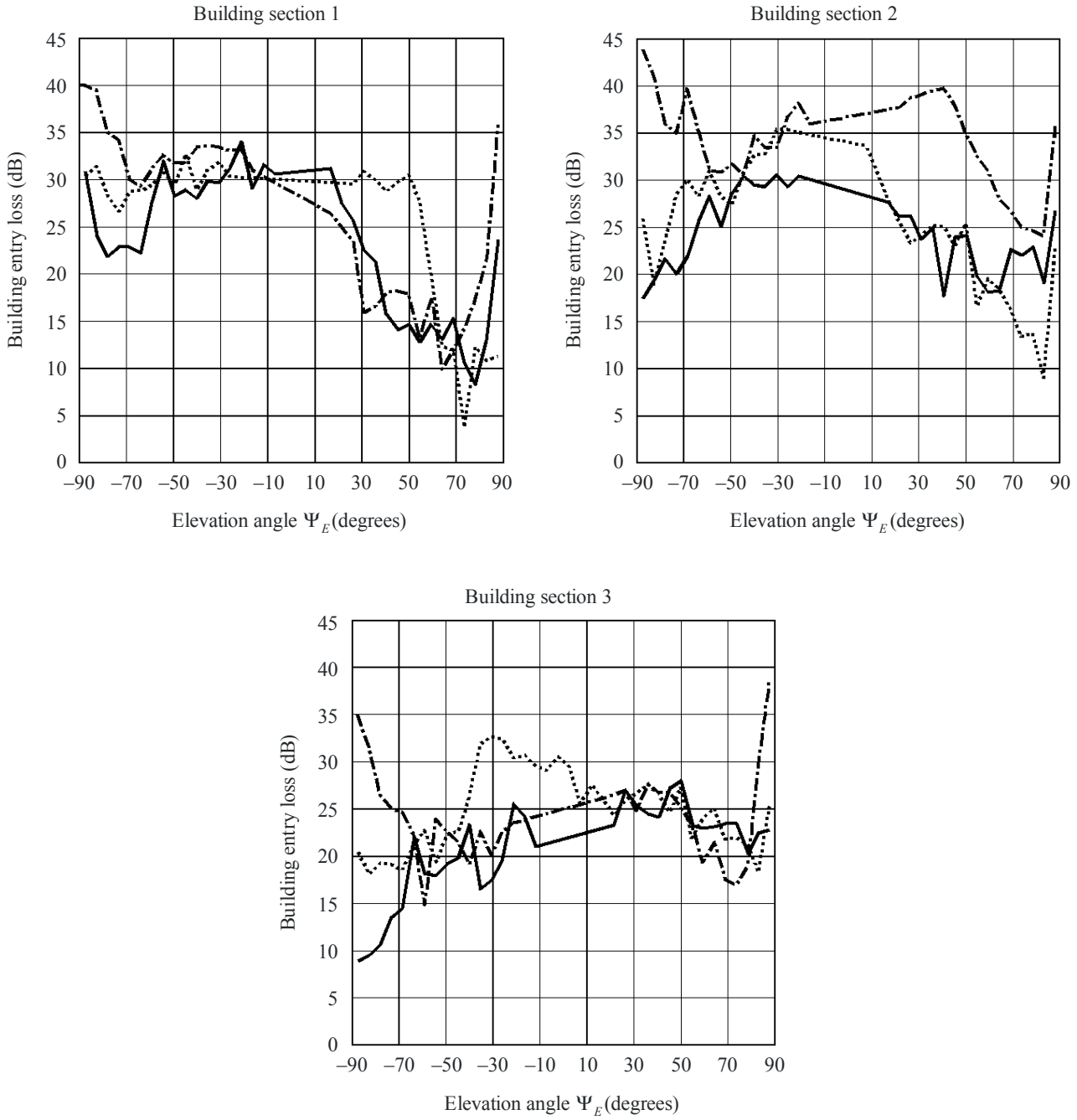

Building section 1: rooms with windows facing helicopter transmitter.

Building section 2: center of corridor.

Building section 3: rooms with windows not facing helicopter transmitter.

P.2040-25

FIGURE 26

Building entry loss at 5.1 GHz for elevation 15° and 30° at the four different indoor antenna positions. Numbers 1 and 2 are located close to an outer wall, whereas numbers 3 and 4 are located in the corridor

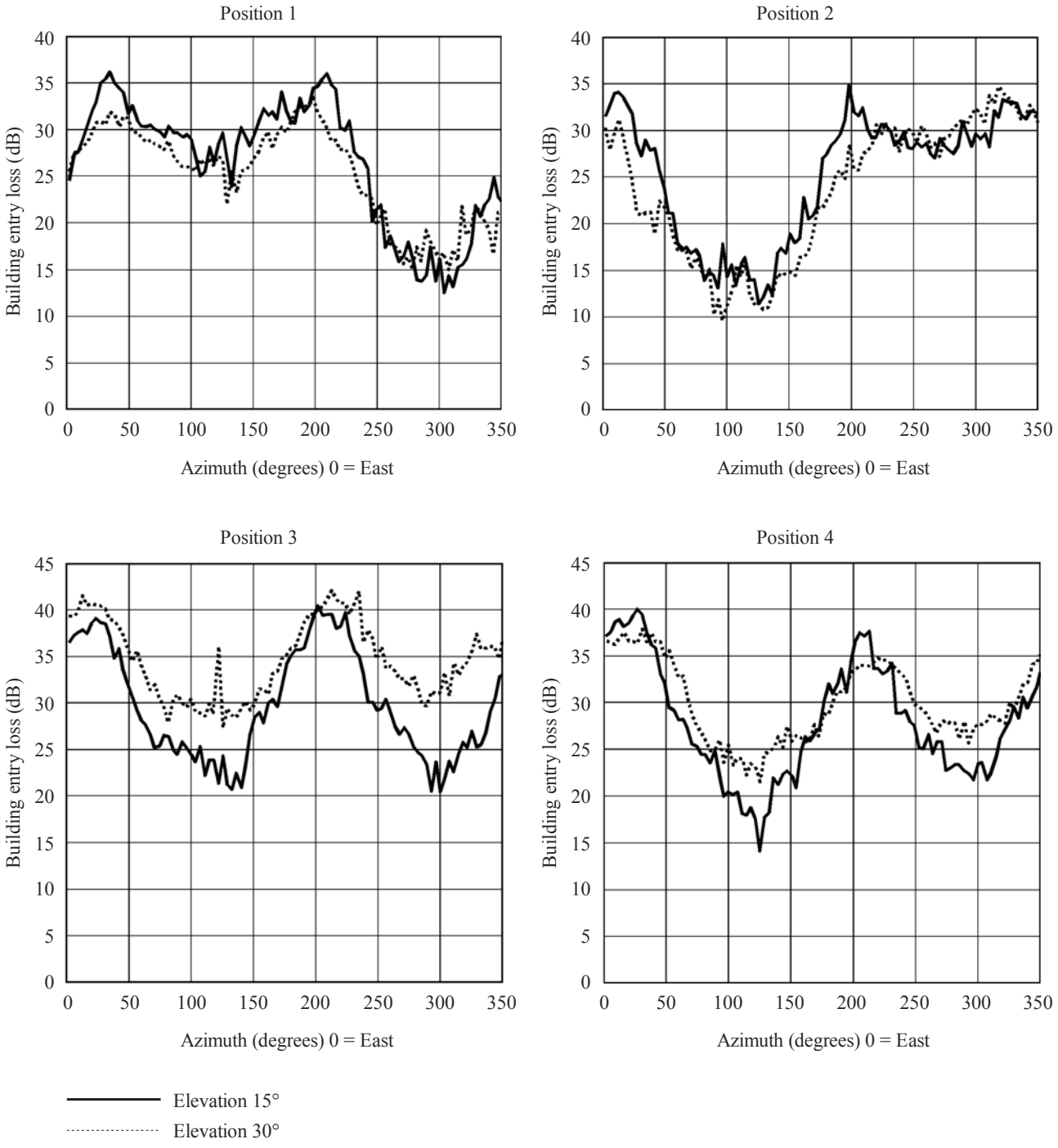

TABLE 9

Average median building entry loss and observed range of the median building entry loss measured at 5.1 GHz for different positions in an office building

	Type of measurements (helicopter trajectory)	Average of the median building entry loss for different receiver positions in the building (dB)	Observed range of the median building entry loss (dB)
Eight-storey building with seven storeys above ground and one extra storey placed on the former roof, brick-walls and windows placed in strips: behind the brick-wall there is a 10 cm thick concrete wall; windows made of two layers of plain non-thermal glass, storeys separated by 3.5 m with 2.5 m from floor to ceiling, two layers of plaster with wooden laths in between separate the rooms; interior walls facing the corridor are in most cases made of glass, rooms commonly furnished with desks and bookshelves; each storey has three sections, a corridor with office rooms at the sides	Elevation angle measurements (linear, perpen-dicular to the long side of the building)	19.1	~ 5-45
	Azimuth angle measurements (circular at elevation angles of 15° and 30°)	22.3	~ 10-42

Measurements at 2.57 GHz and 5.2 GHz using an igloo shaped flight pattern were performed inward to three different buildings, one of them in the Graz/Austria area, another two in the Vienna/Austria area, covering various building types. The transmitter was carried by a helicopter, on which a steerable helix antenna was mounted. The measurements were performed with a high resolution, pseudo random sequence based channel sounder with a chipping rate of 100 Mcps and 200 MHz bandwidth. The transmit antenna was right-hand circularly polarized (RHCP) while the receive antenna for the channel sounder case consisted of a set of patch antennas with two orthogonal linear polarizations covering a surface that approximates a semi-sphere.

Table 10 gives an overview of the inward building locations.

TABLE 10

Overview on buildings measured

Building		Location	#RX locations	Façade/roof material
Millennium Tower skyscraper	22nd floor 44th floor	Vienna	2 2	Metal grid and glass panels, coated glass with sun protective layer/Reinforced concrete
Graz airport	Gate Area Conference room	Feldkirchen near Graz	4 1	Steel, metal construction elements, coated glass with sun protective layer/Steel, metal sheets, layer of gravel
Office building FFG	Inner city office building, highest floor	Vienna	2	Reinforced concrete/coated windows

The building entry loss shown in Table 11 was calculated by subtracting the Average Power Delay Profile from an outdoor reference measurement from the Average Power Delay Profile measurement inside the buildings. The building entry loss for various distances to the window directed to the transmitter at 5.2 GHz is presented in Table 12.

TABLE 11

Entry loss (dB) for different elevation and relative azimuth angles at 2.57 and 5.2 GHz

Building	Relative azimuth to facade normal	2.57 GHz				5.2 GHz			
		Elevation				Elevation			
		15	30	45	60	15	30	45	60
Millennium Tower 44th floor	0	22.86	24.42	21.53	23.95	30.40	27.65	32.09	29.77
	–30	22.13	22.17	25.21	24.59	28.34	30.42	32.43	33.31
	–60	24.44	23.71	25.91	24.60	29.00	31.31	33.57	34.97
	–90	25.40	29.24	27.21	26.77	32.65	34.23	37.24	38.21
Millennium Tower 22nd floor	0	28.04	28.31	28.13	28.28	36.53	37.55	35.38	39.45
	–30	28.70	29.60	29.60	27.59	31.84	36.57	37.51	35.34
	–60	32.26	33.17	33.66	35.38	35.19	37.12	35.90	39.65
	–90	35.30	42.22	37.80	–	43.20	43.80	47.02	46.52
Office Building	0	21.69	29.23	26.18	31.40	26.52	31.13	34.13	35.28
	30	26.49	34.90	31.10	33.00	33.12	33.49	36.51	34.08
	60	27.43	–	35.90	36.13	34.29	34.16	36.30	35.73
	90	–	38.09	–	–	–	–	–	–
Airport – Gate Area	0	18.18	–	23.68	23.00	28.36	35.76	–	37.97
	–30	15.09	21.12	19.11	27.10	–	–	–	37.98
	–60	18.25	26.13	21.96	25.42	27.67	37.76	–	–
	–90	–	27.71	23.69	24.61	34.31	–	–	–

TABLE 11 (*end*)

Entry loss (dB) for different elevation and relative azimuth angles at 2.57 and 5.2 GHz

Building	Relative azimuth to facade normal	2.57 GHz				5.2 GHz			
		Elevation				Elevation			
		15	30	45	60	15	30	45	60
Airport – Conference Room	0	11.81	12.62	–	10.84	15.19	19.68	19.37	19.09
	–30	11.69	–	15.05	13.63	17.73	19.37	20.03	–
	–60	16.65	17.87	17.66	16.35	22.79	–	24.70	22.38
	–90	18.52	20.10	17.43	–	25.17	24.32	23.43	–

TABLE 12

Entry loss (dB) at 5.2 GHz for different elevation angles relative to the distance to the window directed to the transmitter located at 0 degrees relative azimuth angle to the façade normal

Building	Distance to window (m)	Elevation			
		15	30	45	60
Millenium Tower 44th floor	1.4	–	25.30	31.41	27.80
	2.4	–	27.34	31.16	27.81
	3.4	–	29.72	31.64	30.58
	4.4	–	25.6	32.19	28.88
	5.4	30.40	29.08	33.43	30.34
Airport – Gate Area	0.5	30.63	35.07	–	38.72
	2.5	30.28	35.01	–	37.09
	4.5	29.97	35.96	–	38.03
	6.5	16.40	36.85	–	–

4.1.3.4 Balloon measurements to domestic buildings (1-6 GHz)

Measurements have been made in the United Kingdom of building entry loss into a number of domestic buildings of traditional construction. These measurements were made at 1.4 GHz, 2.4 GHz and 5.8 GHz, and used a tethered balloon to explore a range of elevation angles.

Details of measurement locations are given in Table 13.

TABLE 13

Building	Date	Measurement locations
Small offices/flats (3 floors)	1985	Measurements in two offices (1st floor)
Detached house (3 floors)	1905	Kitchen (Ground) and bedroom (1st floor)
Terraced house (2 floors and attic)	1880	Living room (Ground), Bedroom (1st floor) and study (2nd floor)
Terraced house (2 floors)	1965	Dining room & living room (Ground), hallway (1st floor)

The measurements were made using CW transmitters suspended from a tethered helium balloon, which allowed elevation angles up to around 70º to be explored. The receiver was switched between an indoor measuring antenna and an external reference antenna. The measuring antenna was moved along a 1 m track under computer control, to allow spatial averaging of measurements.

Omnidirectional antennas were used at both transmitter and receiver, and corrections were applied for antenna vertical radiation patterns, and the difference in free-space loss between the reference and measuring antennas.

Following the corrections described above, a data set giving the mean penetration loss for each test location was obtained. The cumulative distribution function of these results is shown in Fig. 27, and represents the statistics of mean local loss with respect to all 11 receiver locations, at all elevation angles. The receiver locations were randomly chosen and were almost entirely NLoS to the balloon.

FIGURE 27

Overall statistics of building penetration loss

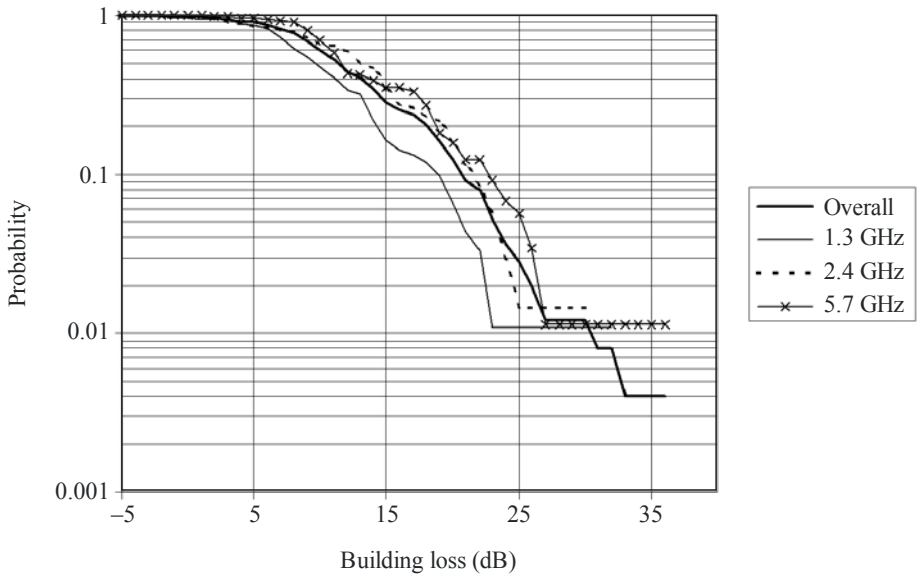

P.2040-27

The mean value of building penetration loss, at all frequencies, is 11.2 dB. The results shown in Fig. 27 show a slight frequency dependence in the results. Mean values of penetration loss are 9.2 dB at 1.3 GHz, 11.2 dB at 2.4 GHz and 12.7 dB at 5.7 GHz.

Figure 28 shows the elevation dependence of the measurements (polynomial curves fitted to measurement points).

FIGURE 28

Mean values for each frequency compared

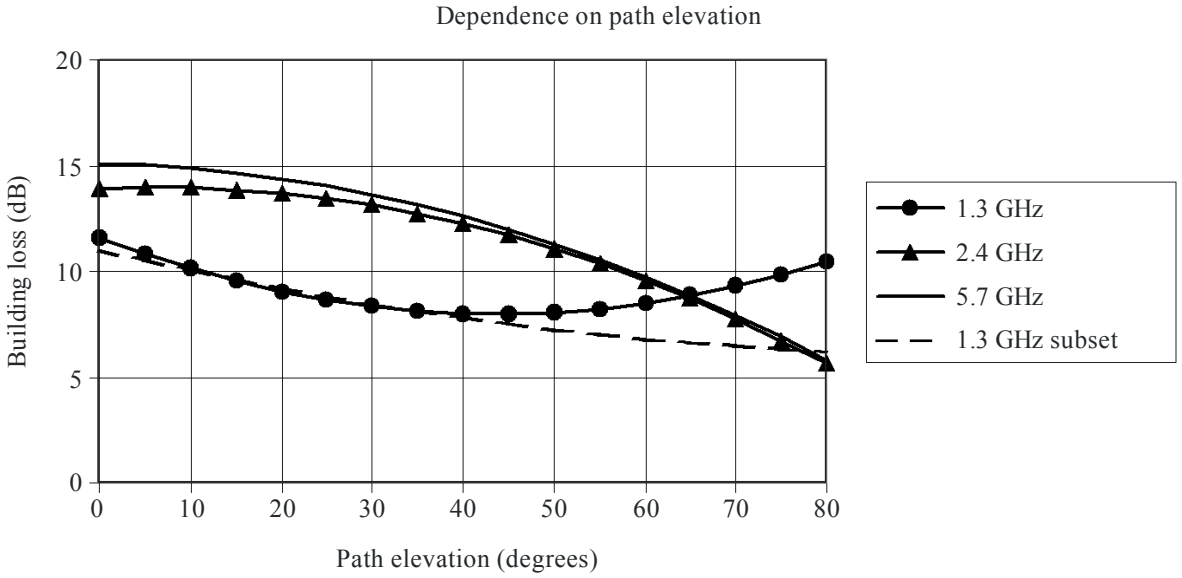

P.2040-28

The results at 1.3 GHz show an anomalous increase in the penetration loss for higher elevation angles. Examination of the measurement data shows that this effect is due to one set of measurements and the effect of excluding this data is shown in the dotted curve.

It can be seen that, except at the lowest frequency, there is a slight decrease in penetration loss for higher elevation angles. This decrease in building loss with elevation runs counter to the assumptions made in some previous models. It may be that this behaviour is characteristic of domestic buildings, where floors and ceilings are typically of light wooden construction.

Some dependence, of the averaged results, on the building floor is apparent, with the ground floor and first floor results generally showing some 5-8 dB greater loss than those for the second floor. It should be borne in mind, however, that only one set of measurements was made on a second floor, and the location was a converted roof space, used as a home office.

4.2 Losses within buildings

Studies of terrestrial propagation within buildings indicate that at 2 GHz in an office building, the loss (dB) though floors is given by $15 + 4(n - 1)$ where n is the number of floors penetrated. For a residential building, the loss is typically 4 dB per floor, which serves to estimate the additional loss of a satellite signal entering from a high elevation angle and passing downwards through a building.

4.3 Building exit loss measurements

4.3.1 Measurement configuration

Figure 29 shows a picture of the house used in the measurement. It is a typical bi-level frame house in Japan. The site is approximately 11 m × 12 m. The outer walls have two or three windows on each side. The outside of the exterior walls is covered by painted wooden boards and the inside of the walls are covered with plasterboard. Glass fibre insulation fills the space between inside the

walls. A transmitting antenna is set near the centre of the lower floor. The antenna height above the floor level is 1.5 m. A 5.2-GHz continuous wave is transmitted from a vertically polarized dipole antenna. A receiver connected to a dipole antenna is set on a pushcart and moved around the house. The receiving antenna height is set at 2.2 m from the ground level to make it equal in height to the transmitting antenna. Before conducting outside measurements, the received level is measured at several points inside the house.

4.3.2 Measured result

Figure 30 is a contour map of the received level. High levels are expressed as dark colour and low levels are expressed as light colours. The map shows that intense radiowaves spread out through the windows and propagate to relatively far distances. In this figure, the white part in the upper right corner indicates the location where we could not take measurements due to a barn. The other white part in the upper left side is due to a hedgerow.

FIGURE 29

Photo of house

P.2040-29

FIGURE 30

Contour map of the received level

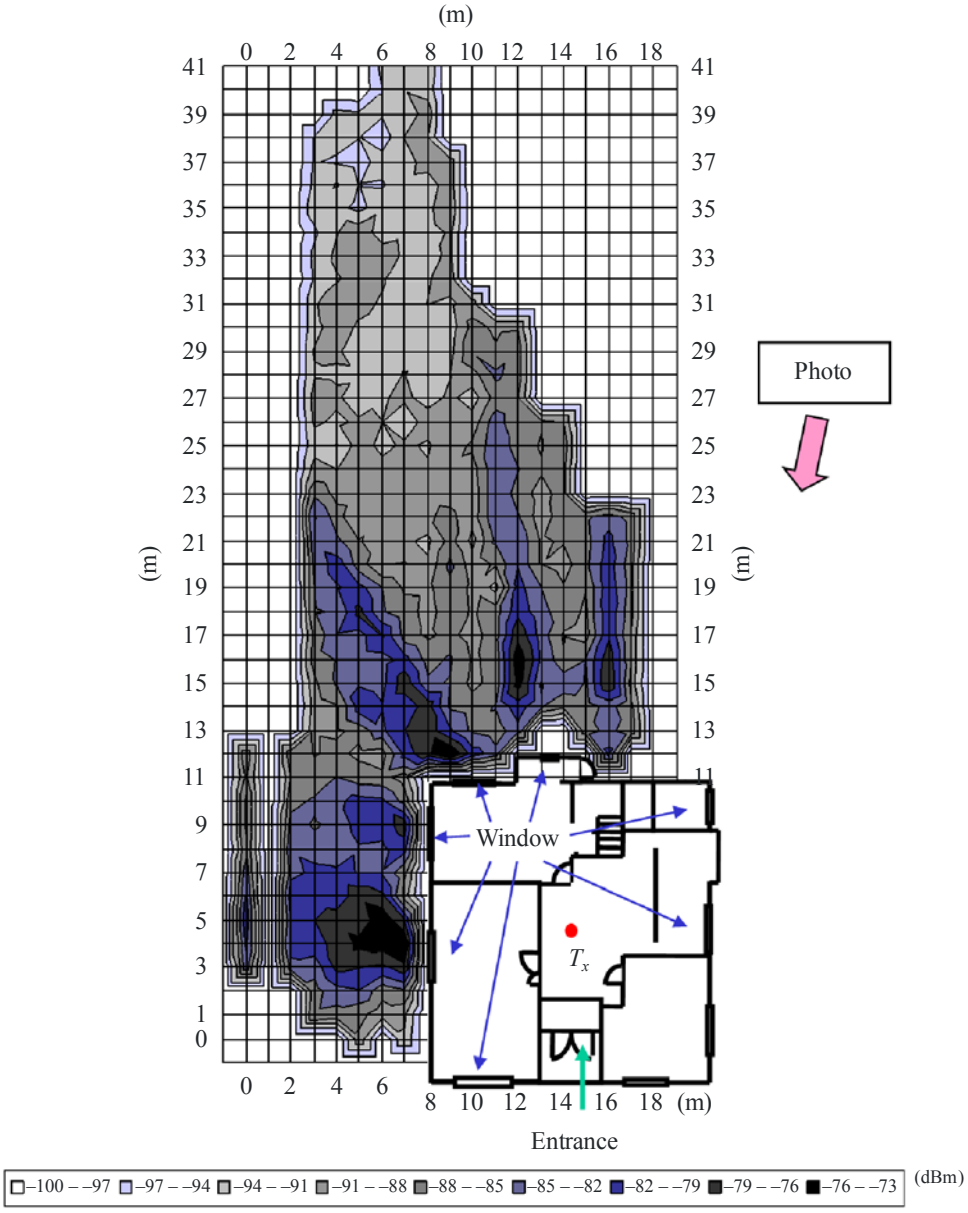

P.2040-30

Figure 31 shows the distance dependency of the path loss. The abscissa is a linear scale. The blue circles represent outdoor data and the red triangles represent indoor data. The path loss is approximated by the following equation.

$$L(\text{dB}) = 20\log(f(\text{MHz})) + N\log(d(\text{m})) - 27.55 + L_f(\text{dB}) \quad (91)$$

where N is the attenuation coefficient for distance and L_f is the additional attenuation caused by wall penetration for example. When N and L_f equal 20 and 0, respectively, this equation expresses the free-space path loss.

Three calculated lines are shown in Fig. 31. The black dashed line is the free-space path loss at 5.2 GHz. The red solid line approximates the indoor data set. Its L_f equals zero but N equals 30 for a large decline compared to that for free space. The blue solid line has $N = 20$ and $L_f = 15$. The curve parallels that for free-space curve but with a drop of 15 dB. This result indicates that the path loss increases with a large N within the house and the increase becomes gradual after it exits the house. This feature is clearly observed in Fig. 31.

FIGURE 31

Distance dependencies of the path loss (linear scale)

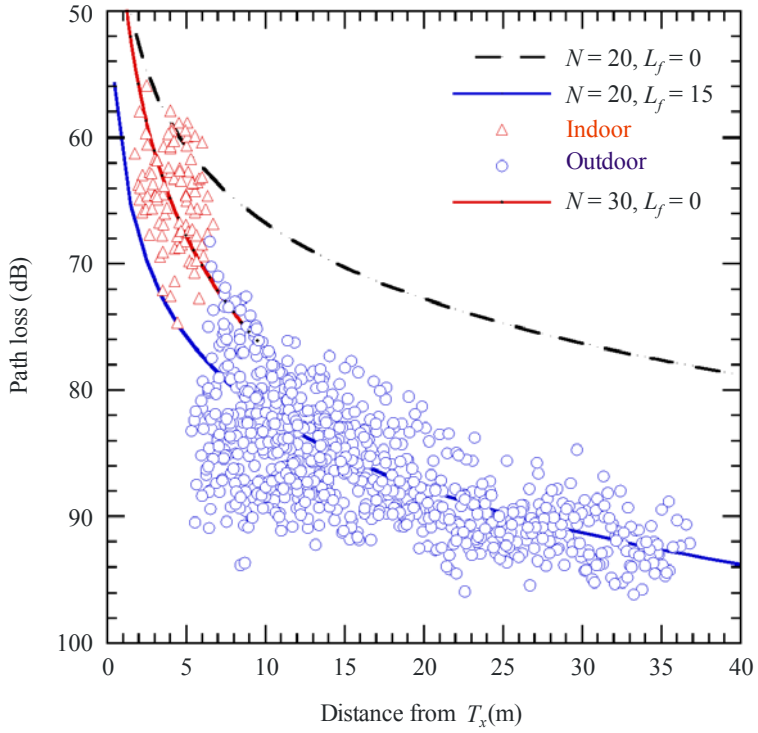

P.2040-31

Based on these data, cumulative probabilities of the path loss are derived in Fig. 32. The difference between these two probabilities is approximately 18 dB. This indicates that the radiowave exits from the house with an attenuation of approximately 18 dB and propagates with the same attenuation coefficient in distance as that for free space.

FIGURE 32

Cumulative probabilities of measured path loss data

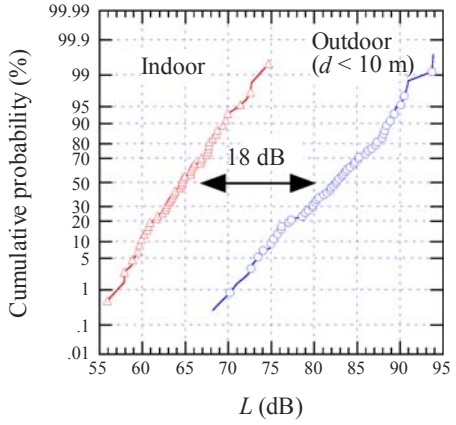

P.2040-32

4.4 Building shadowing loss measurements

Measurements have been carried out in Australia to determine values of building shadowing loss to be used in planning frequency sharing between the fixed-satellite service and the fixed service.

The building shadowing loss is defined as transmission loss through a building.

The frequency is 11 GHz. Polarization is vertical and horizontal.

Table 14 shows the average results of measurements at 11 GHz through the different types of buildings.

TABLE 14

Mean and standard deviation of loss by polarization and building type

Test site		Avg. loss (V-Pol)	Std. dev.	Avg. loss (H-Pol)	Std. dev.
1.	Wooden building (lengthways)	26.4 dB	7.1	–	-
1A.	Wooden building (widthways)	10.0 dB	7.0	8.3 dB	5.0
2.	Concrete/brick building	30.1 dB	5.0	28.6 dB	5.5
3.	Metal shed	36.4 dB	4.1	35.0 dB	3.2

The measurements show a high dependence on construction material in determining:

– the primary mode of propagation; and

– the amount of attenuation caused by the obstacle.

Wooden construction materials caused the lowest average attenuation of 10.0 to 25.0 dB, brick and concrete between 25.0 and 35.0 dB and metal between 35.0 and 40.0 dB. The primary mode of propagation for wooden and concrete structures was transmission, while the dominant mode of propagation for metal structures was propagation by diffraction.

During propagation by diffraction, there was a high dependence on diffraction angle. As the diffraction angle increased from the corners (i.e. towards the centre of the building shadow) the amount of attenuation due to diffraction increased (on the order of 5.0 to 10.0 dB).

Although there was dependence on polarization at each measurement point, there was little to no dependence on polarization or path length from the standpoint of averaged data. The average attenuation variation between horizontal and vertical polarizations was less than 1.5 dB.

Appendix 1
(to § 2.2.2.2)

Alternative method to obtain reflection and transmission coefficients for building materials represented by *N* dielectric slabs based on ABCD matrix formulation

Alternative formulas for equations (54) to (58) in § 2.2.2.2 are given below to obtain the reflection (R) and transmission (T) coefficients for a building material represented by N dielectric slabs based on the ABCD matrix formulation. The regions on both sides of the building material are assumed to be free space. Note that this alternative method produces exactly the same results as that given in § 2.2.2.2.

$$R_N = \frac{B/Z_N - CZ_N}{2A + B/Z_N + CZ_N} \tag{92a}$$

$$R_P = -\frac{B/Z_P - CZ_P}{2A + B/Z_P + CZ_P} \tag{92b}$$

$$T_N = \frac{2}{2A + B/Z_N + CZ_N} \tag{92c}$$

$$T_P = \frac{2}{2A + B/Z_P + CZ_P} \tag{92d}$$

Here A, B, and C are the elements of the ABCD matrix given by:

$$\begin{bmatrix} A & B \\ C & D \end{bmatrix} = \begin{bmatrix} A_1 & B_1 \\ C_1 & D_1 \end{bmatrix} \cdots \begin{bmatrix} A_m & B_m \\ C_m & D_m \end{bmatrix} \cdots \begin{bmatrix} A_N & B_N \\ C_N & D_N \end{bmatrix} \tag{93a}$$

where:

$$A_m = \cos(\beta_m d_m) \tag{93b}$$

$$B_m = jZ_m \sin(\beta_m d_m) \tag{93c}$$

$$C_m = \frac{j \sin(\beta_m d_m)}{Z_m} \tag{93d}$$

$$D_m = A_m \tag{93e}$$

$$\beta_m = k_m \cos(\theta_m) = k_m \left[1 - \left(\frac{\eta_0}{\eta_m} \sin\theta_0 \right)^2 \right]^{1/2} \tag{93f}$$

$$k_0 = \frac{2\pi}{\lambda} \tag{93g}$$

$$k_m = k_0 \sqrt{n_m} \tag{93h}$$

In equations (93b)-(93h), λ is the free-space wavelength, k_0 is the free-space wave number, η_m and k_m are the complex permittivity and wave number in the m-th slab, β_m is the propagation constant in the direction perpendicular to the slab plane, and d_m is the width of the m-th slab.

The wave impedances Z_N and Z_P for E-fields perpendicular and parallel to the reflection plane are given by:

$$Z_N = \chi_m / \cos\theta_m \tag{94a}$$

and:

$$Z_P = \chi_m \cos\theta_m \tag{94b}$$

where χ_m is the intrinsic impedance of the m-th slab given by:

$$\chi_m = \frac{120\pi}{\sqrt{\eta_m}} \tag{94c}$$

where:

$$\eta_0 = \eta_{N+1} = 1 \tag{94d}$$

$$\theta_0 = \theta_{N+1} = \theta \tag{94e}$$

$$Z_0 = Z_{N+1} \tag{94f}$$